

1                   **Response of the Global Surface Ozone Distribution to**  
2                   **Northern Hemisphere Sea Surface Temperature Changes:**  
3                   **Implications for Long-Range Transport**  
4

5                   **Kan Yi<sup>1</sup>, Junfeng Liu<sup>1</sup>, George Ban-Weiss<sup>2</sup>, Jiachen Zhang<sup>2</sup>,**  
6                   **Wei Tao<sup>1</sup>, Shu Tao<sup>1</sup>**  
7

8 [1] Laboratory for Earth Surface Processes, College of Urban and Environmental  
9 Sciences, Peking University, Beijing, China  
10

11 [2] Sonny Astani Department of Civil and Environmental Engineering, University of  
12 Southern California, U.S.A.  
13

14 Correspondence to: Junfeng Liu (E-mail: [jfliu@pku.edu.cn](mailto:jfliu@pku.edu.cn))  
15  
16  
17

18 **Abstract**

19 The response of surface ozone (O<sub>3</sub>) concentrations to basin-scale warming and cooling  
20 of Northern Hemisphere oceans is investigated using the Community Earth System  
21 Model (CESM). Idealized, spatially uniform sea surface temperature (SST) anomalies  
22 of +/- 1 °C are individually superimposed onto the North Pacific, North Atlantic, and  
23 North Indian Oceans. Our simulations suggest large seasonal and regional variability  
24 of surface O<sub>3</sub> in response to SST anomalies, especially in the boreal summer. The  
25 responses of surface O<sub>3</sub> associated with basin-scale SST warming and cooling have  
26 similar magnitude but are opposite in sign. Increasing the SST by 1 °C in one of the  
27 oceans generally decreases the surface O<sub>3</sub> concentrations from 1 to 5 ppbv. With fixed  
28 emissions, SST increases in a specific ocean basin in the Northern Hemisphere tend to  
29 increase the summertime surface O<sub>3</sub> concentrations over upwind regions, accompanied  
30 by a widespread reduction over downwind continents. We implement the integrated  
31 process rate (IPR) analysis in CESM and find that meteorological O<sub>3</sub> transport in  
32 response to SST changes is the key process causing surface O<sub>3</sub> perturbations in most

33 cases. During the boreal summer, basin-scale SST warming facilitates the vertical  
34 transport of O<sub>3</sub> to the surface over upwind regions while significantly reducing the  
35 vertical transport over downwind continents. This process, as confirmed by tagged CO-  
36 like tracers, indicates a considerable suppression of intercontinental O<sub>3</sub> transport due to  
37 increased tropospheric stability at lower mid-latitudes induced by SST changes. On the  
38 other hand, the responses of chemical O<sub>3</sub> production to regional SST warming can exert  
39 positive effects on surface O<sub>3</sub> levels over highly polluted continents, except South Asia,  
40 where intensified cloud loading in response to North Indian SST warming depresses  
41 both the surface air temperature and solar radiation, and thus photochemical O<sub>3</sub>  
42 production. Our findings indicate a robust linkage between basin-scale SST variability  
43 and continental surface O<sub>3</sub> pollution, which should be considered in regional air quality  
44 management.

45

46 **Keywords:** SST anomaly, Surface O<sub>3</sub>, Process analysis, Transport, CESM

47

48

## 49 **1. Introduction**

50 High ground-level ozone (O<sub>3</sub>) concentrations adversely impact human health by  
51 inducing respiratory diseases and threaten food security by lowering crop yields  
52 (Brown and Bowman, 2013; WHO, 2013; Chuwah et al., 2015). Considering the eco-  
53 toxicity of O<sub>3</sub>, understanding the physical and chemical mechanisms that control  
54 atmospheric O<sub>3</sub> concentrations is of great importance. Surface O<sub>3</sub> is produced in the  
55 atmosphere via photochemical processing of multiple precursors including volatile  
56 organic compounds (VOCs), carbon monoxide (CO) and nitrogen oxides (NO, NO<sub>2</sub>).  
57 These precursors originate from both natural and anthropogenic sources (Vingarzan,  
58 2004; Simon et al., 2014; Jiang et al., 2016). In addition to local production, transport  
59 of O<sub>3</sub> and its precursors from upwind regions and the upper atmosphere can also  
60 influence surface O<sub>3</sub> abundance. Stratospheric intrusion events, which lead to vertical  
61 down-mixing of ozone-rich air, can significantly elevate surface O<sub>3</sub> during spring

62 (Grewe, 2006; Lin et al., 2012b; Zhang et al., 2014). The long-range transport of O<sub>3</sub>  
63 and its precursors has been extensively studied, and their inter-continental impacts have  
64 been evaluated using measurements and model simulations (Parrish et al., 1993;  
65 Fehsenfeld et al., 1996; Wild and Akimoto, 2001; Creilson et al., 2003; Simmonds et  
66 al., 2004; Fiore et al., 2009; Brown-Steiner and Hess, 2011; Lin et al., 2012a; Lin et al.,  
67 2014).

68

69 Both photochemistry and dynamic transport collectively affect surface O<sub>3</sub> levels.  
70 Important meteorological factors that can impact both photochemistry and transport  
71 include atmospheric circulations, solar radiation, air temperature, and relative humidity.  
72 Atmospheric circulation considerably determines the timescale and pathway of O<sub>3</sub>  
73 transport (Bronnimann et al., 2000; Auvray and Bey, 2005; Hess and Mahowald, 2009).  
74 The efficiency of O<sub>3</sub> transport varies coherently with atmospheric circulations on  
75 different scales. Knowland et al. (2015) demonstrated the important role of mid-latitude  
76 storms in redistributing O<sub>3</sub> concentrations during springtime. The North Atlantic  
77 Oscillation (NAO) significantly affects surface and tropospheric O<sub>3</sub> concentrations over  
78 most of Europe by influencing the intercontinental transport of air masses (Creilson et  
79 al., 2003; Christoudias et al., 2012; Pausata et al., 2012). Lamarque and Hess (2004)  
80 indicated that the Arctic Oscillation (AO) can modulate springtime tropospheric O<sub>3</sub>  
81 burdens over North America. The shift in the position of the jet stream associated with  
82 climate change was found to strongly affect summertime surface O<sub>3</sub> variability over  
83 eastern North America (Barnes and Fiore, 2013). Increases in solar radiation and air  
84 temperature can increase the rate of the chemical production of O<sub>3</sub> and modulate the  
85 biogenic emissions of O<sub>3</sub> precursors (Guenther, 1993; Sillman and Samson, 1995;  
86 Peñuelas and Llusà, 2001), especially over highly polluted regions (Ordóñez et al.,  
87 2005; Rasmussen et al., 2012; Pusede et al., 2015). Increases in humidity can enhance  
88 the chemical destruction of O<sub>3</sub> and shorten its atmospheric lifetime (Johnson et al., 1999;  
89 Camalier et al., 2007). Therefore, changes in meteorological conditions on various  
90 spatial and temporal scales play key roles in determining the surface O<sub>3</sub> distribution.  
91 Understanding the mechanisms and feedbacks of the interactions between O<sub>3</sub> and

92 climate has received increasing attention and will be essential for future surface O<sub>3</sub>  
93 mitigation (Jacob and Winner, 2009; Doherty et al., 2013).

94

95 Sea surface temperature (SST) is an important indicator that characterizes the state of  
96 the climate system. Its variations strongly perturb the mass and energy exchange  
97 between the ocean and atmosphere (Small et al., 2008; Gulev et al., 2013), which  
98 influence atmospheric circulation, atmospheric temperature and specific humidity  
99 (Sutton and Hodson, 2005; Frankignoul and Sennéchaël, 2007; Li et al., 2008) from  
100 regional to global scales (Glantz et al., 1991; Wang et al., 2000; Goswami et al., 2006).  
101 It also affects cloud formation and consequently influences incoming solar radiation  
102 (Deser et al., 1993; Fallmann et al., 2017). Numerous studies have shown that SST  
103 changes over different oceans and at different latitudes lead to significantly different  
104 meteorological and climate responses (Webster, 1981; Lau and Nath, 1994; Lau, 1997;  
105 Sutton and Hodson, 2007; Sabeerali et al., 2012; Ueda et al., 2015). Details on the SST-  
106 climate relationships over individual oceanic regions are summarized in Kushnir et al.  
107 (2002).

108

109 The Intergovernmental Panel on Climate Change Fifth Assessment Report (IPCC, 2013)  
110 provides strong evidences in Chapter 2 that global SSTs are generally increasing due to  
111 the impacts of anthropogenic forcings on global climate change. In addition, regional  
112 SST exhibits natural periodic or irregular oscillations with timescales ranging from  
113 months to decades. The El Niño/Southern Oscillation (ENSO) is the most influential  
114 natural SST variability that originates in the tropical Pacific and has worldwide climate  
115 impacts (Philander, 1983; Wang et al., 2012). The Pacific decadal oscillation (PDO),  
116 defined by ocean temperature anomalies in the northeast and tropical Pacific Ocean, is  
117 another long-lived, El Niño-like pattern that persists for several decades (Mantua and  
118 Hare, 2002). Over the Indian Ocean, SST anomalies feature a seesaw structure between  
119 the western and eastern equatorial regions, known as the Indian Ocean Dipole (IOD)  
120 mode (Saji et al., 1999). The North Atlantic Ocean exhibits various modes of low-  
121 frequency SST variability (Kushnir, 1994; Wu and Liu, 2005; Fan and Schneider, 2012;

122 Taboada and Anadon, 2012). The mechanisms responsible for SST variability includes  
123 ocean circulation variability, wind stress, and ocean-atmosphere feedbacks  
124 (Frankignoul, 1985; Deser et al., 2010). Aerosols and greenhouse gases (GHGs)  
125 emitted from anthropogenic and natural sources also contribute to regional SST  
126 variability through modulation of the solar radiation received by the ocean surface  
127 (Rotstayn and Lohmann, 2002; Wu and Kinter, 2011; Hsieh et al., 2013; Ding et al.,  
128 2014; Meehl et al., 2015).

129

130 Considering the distinct roles of regional SST variability in modulating regional climate  
131 systems, the impact of regional SST changes on the surface O<sub>3</sub> distribution needs to be  
132 explored. Lin et al. (2015) found that more frequent deep stratospheric intrusions appear  
133 over the western US during strong La Niña springs because of the meandering of the  
134 polar jet towards this region. This process can remarkably increase surface O<sub>3</sub> levels in  
135 the western US. The La Niña-like decadal cooling of the eastern equatorial Pacific  
136 Ocean in the 2000s weakened the long range transport of O<sub>3</sub>-rich air from Eurasia  
137 towards Hawaii during spring (Lin et al., 2014). Liu et al. (2005) revealed that El Niño  
138 winters are associated with stronger transpacific pollutant transport, which also has  
139 implications for the long-range transport of O<sub>3</sub>. Except for the ENSO impacts, very few  
140 studies to date have directly addressed the linkage between SST and O<sub>3</sub>. Therefore, a  
141 comprehensive understanding of the response of surface O<sub>3</sub> to SST changes in  
142 individual ocean basins is lacking and necessary.

143

144 To fill this gap, this study focuses on examining the sensitivity of O<sub>3</sub> evolution over  
145 four polluted continental regions in the Northern Hemisphere (i.e., North America (NA,  
146 15°N–55 °N; 60°W–125°W), Europe (EU, 25°N–65 °N; 10°W–50 °E), East Asia (EA,  
147 15 °N–50 °N; 95°E–160 °E) and South Asia (SA, 5 °N–35 °N; 50 °E–95°E), defined  
148 in Fiore et al. (2009)) with respect to nearby basin-scale SST changes. We describe the  
149 design of numerical experiments and model configuration in Section 2. Surface O<sub>3</sub>  
150 responses to regional SST changes are given in Section 3. Relevant mechanisms  
151 governing the SST-O<sub>3</sub> relationships are discussed in Section 4. The impact of basin-

152 scale SST changes on inter-continental transport of O<sub>3</sub> is described in Section 5.  
153 Conclusions are drawn in Section 6.

## 154 **2. Methodology**

### 155 **2.1 Model description and configuration**

156 The Community Earth System Model (CESM, v1.2.2) developed by the National  
157 Center for Atmospheric Research (NCAR) is used in this study, configured with the  
158 Community Atmosphere Model version 5.0 (CAM5) and the Community Land Model  
159 version 4.0 (CLM4). The ocean and sea ice components are prescribed with  
160 climatological SST and sea ice distributions. Moist turbulence is parameterized  
161 following the Bretherton and Park (2009) scheme. Shallow convection is parameterized  
162 using the Park and Bretherton (2009) scheme. The parameterization of deep convection  
163 is based on Zhang and McFarlane (1995) with modifications following Richter and  
164 Rasch (2008), Raymond and Blyth (1986), and Raymond and Blyth (1992). The cloud  
165 microphysical parameterization is following a two-moment scheme described in  
166 Morrison and Gettelman (2008) and Gettelman et al. (2008). The microphysical effect  
167 of aerosols on clouds are simulated following Ghan et al. (2012). The parameterization  
168 of cloud macrophysics follows Conley et al. (2012).

169

170 The chemistry coupled in the CAM5 (i.e., CAM5-chem) is primarily based on the  
171 Model for O<sub>3</sub> and Related chemical Tracers, version 4 (MOZART-4), which resolves  
172 85 gas-phase species, and 196 gas-phase reactions (Emmons et al., 2010; Lamarque et  
173 al., 2012). A three-mode (i.e., Aitkin, accumulation and coarse) aerosol scheme for  
174 black carbon (BC), primary organic matter (POM), second organic aerosol (SOA), sea  
175 salt, dust and sulfate was used in our simulations following Liu and Ghan (2010). The  
176 lightning parameterization is modified according to Price et al. (1997) and tropospheric  
177 photolysis rates are calculated interactively following Tie et al. (2005). Gaseous dry  
178 deposition is calculated using the resistance-based parameterization of Wesely (1989),  
179 Walmsley and Wesely (1996), and Wesely and Hicks (2000). The parameterizations of  
180 in-cloud scavenging and below-cloud washout for soluble species are described in

181 detail by Giorgi and Chameides (1985) and Brasseur et al. (1998), respectively.  
182 Anthropogenic emissions of chemical species are from the IPCC AR5 emission datasets  
183 (Lamarque et al., 2010), whose injection heights and particle size distributions follow  
184 the AEROCOM protocols (Dentener et al., 2006). The emissions of natural aerosols  
185 and precursor gases are prescribed from the MOZART-2 (Horowitz et al., 2003) and  
186 MOZART-4 (Emmons et al., 2010) datasets. All emission datasets are available from  
187 the CESM data inventory (<https://svn-ccsm-inputdata.cgd.ucar.edu/trunk/inputdata/>).  
188 The performance of CESM in simulating tropospheric O<sub>3</sub> has been validated by  
189 comparing with ozonesondes and satellite observations (Tilmes et al., 2014). The  
190 deviations between model and observations are within the range of about 25%. In  
191 general, the model can capture the surface ozone distribution and variability well, but  
192 may overestimate O<sub>3</sub> over the Eastern US and Western Europe in the summer (Tilmes  
193 et al., 2014).

194

## 195 **2.2 Numerical experiments**

196 We first conduct a control simulation, hereafter referred to as CTRL, with prescribed  
197 climatological monthly SSTs averaged from 1981 to 2010 (see Hurrell et al. (2008)).  
198 We then conduct six perturbation simulations with monthly SSTs that are uniformly  
199 increased or decreased by 1°C in three ocean basins in the Northern Hemisphere: the  
200 North Pacific (15°N-65°N; 100°E-90°W), North Atlantic (15°N-65°N; 100°W-20°E)  
201 and North Indian Oceans (5°N-30°N, 30°E-100°E; here 5°N is used to attain a relatively  
202 larger domain size). The simulations are denoted as “Pacific-W”, “Atlantic-W” and  
203 “Indian-W” for the three warming cases and “Pacific-C”, “Atlantic-C” and “Indian-C”  
204 for the three cooling cases. We defined the latitudinal and longitudinal ranges of these  
205 ocean basins mainly based on their geographical features. The boundaries of the  
206 prescribed SST anomalies generally align with the edge of the ocean basins, except  
207 along the southern side. In each perturbation simulation, we linearly smooth the  
208 southern boundaries of these SST anomalies towards the equator to remove the sharp  
209 SST anomaly gradients at the edge, following a previous approach (e.g., Taschetto et  
210 al., 2016; Seager and Henderson, 2016). We further conduct two sensitivity tests with

211 1 °C SST warming and 1 °C SST cooling superimposed onto all three ocean basins (i.e.,  
212 the North Pacific, North Atlantic and North Indian Ocean) in the Northern Hemisphere,  
213 denoted as “All-W” and “All-C”, respectively. Air pollution emissions, including  
214 biogenic emissions of VOCs, are fixed to distinguish the impacts of SST variation on  
215 O<sub>3</sub> transport and photochemistry. All simulations are run for 21 years with the first year  
216 used for model spin-up.

217

218 To explore the impacts of SST changes on inter-continental transport, an explicit  
219 emission tagging technique is used in our simulations following previous studies  
220 (Shindell et al., 2008; Doherty et al., 2013). Artificial CO-like tracers emitted from four  
221 continental regions, i.e., North America (NA, 15°N–55 °N; 60°W–125°W), Europe  
222 (EU, 25°N–65 °N; 10°W–50 °E), East Asia (EA, 15 °N–50 °N; 95°E–160 °E) and South  
223 Asia (SA, 5 °N–35 °N; 50 °E–95°E), are tracked individually. These tracers are  
224 idealized with a first-order decay lifetime of 50 days, which is similar to O<sub>3</sub> (Doherty  
225 et al., 2013) and used to single out changes in O<sub>3</sub> transport induced by SST anomalies.

226

### 227 **2.3 Integrated process rate (IPR) analysis**

228 To provide a process-level explanation for the response of surface O<sub>3</sub> to regional SST  
229 changes, the IPR method is applied. This method calculates the accumulated  
230 contributions of individual processes (e.g., chemical production and loss, advection,  
231 vertical diffusion, dry deposition, etc.) to O<sub>3</sub> predictions during the model simulation  
232 and has been widely used for air pollution diagnostics (Li et al., 2012; Zhang and Wu,  
233 2013; Tao et al., 2015). In this study, we added the IPR scheme to the CESM framework  
234 to track the contribution of six physicochemical processes (i.e., gas-phase chemistry  
235 (CHEM), advection (ADVE), vertical diffusion (VDIF), dry deposition (DRYD),  
236 shallow convection (SHAL) and deep convection (DEEP)) to O<sub>3</sub> concentrations in  
237 every grid box. Wet deposition and aqueous-phase chemistry are ignored here due to  
238 the low solubility and negligible chemical production of O<sub>3</sub> in water (Jacob, 1999).  
239 Therefore, CHEM represents the net production (production minus loss) rate of O<sub>3</sub> due  
240 to gas-phase photochemistry. DRYD represents the dry deposition fluxes of O<sub>3</sub>, which

241 is an important sink for O<sub>3</sub>. The other IPR terms (i.e., ADVE, VDIF, SHAL and DEEP)  
242 represent contributions from different transport processes. The IPR scheme tracks and  
243 archives the O<sub>3</sub> flux in each grid from every process during each model time step. The  
244 sum of the O<sub>3</sub> fluxes from these six processes matches the change in the O<sub>3</sub>  
245 concentration. The IPR method has been widely used in air quality studies to examine  
246 the cause of pollution episodes (Wang et al., 2010; Li et al., 2012). When applied in  
247 climate sensitivity analysis (usually measuring the difference between two  
248 equilibriums), the net change of all IPRs approaches zero. Typically, the positive  
249 changes in IPRs are mainly responsible for the increase in surface O<sub>3</sub>, which may  
250 further induce O<sub>3</sub> removal to balance this forcing in a new equilibrium. Therefore, here,  
251 the IPR analysis is used not to budget the SST-induced O<sub>3</sub> concentration changes but  
252 rather to help examine the relative importance of different transport and chemical  
253 processes in driving the sensitivity of O<sub>3</sub> to SST forcing. Its performance is verified by  
254 comparing the predicted hourly O<sub>3</sub> changes with the sum of the individual fluxes from  
255 the six processes. As shown in Figure S1, the hourly surface O<sub>3</sub> changes are well  
256 represented by the sum of these fluxes in the model.

257

### 258 **3. Response of surface O<sub>3</sub> concentrations to SST changes**

259 Seasonally and regionally averaged surface O<sub>3</sub> changes in each SST perturbation  
260 simulation for the four highly populated continental regions and three ocean basins  
261 defined in our study are given in Tables 1 and S1, respectively. The responses of the  
262 surface O<sub>3</sub> concentrations to basin-scale SST changes (i.e.,  $\pm 1$  °C) are mainly below  
263 3 ppbv in the Northern Hemisphere (Tables 1 and S1), though larger anomalies (i.e., up  
264 to 5 ppbv) are also observed over the eastern coast of China, the Indian subcontinent,  
265 and certain oceanic areas (Figures 1 and S2). This SST-O<sub>3</sub> sensitivity is comparable to  
266 previous findings. For instance, Bloomer et al. (2009) reported a positive O<sub>3</sub>-  
267 temperature relationship of 2.2~3.2 ppbv/°C across the rural eastern United States. Wu  
268 et al. (2008) found that summertime surface O<sub>3</sub> may increase by 2-5 ppbv over the  
269 northeastern United States in the 2050s. Additionally, Fiore et al. (2009) demonstrated

270 an intercontinental decrease in surface O<sub>3</sub> of no more than 1 ppbv in response to 20 %  
271 reductions in anthropogenic emissions within a continental region. Our study indicates  
272 that basin-scale SST changes alone may exert significant effects on the surface O<sub>3</sub>  
273 above specific ocean basin and its surrounding continents.

274

275 As shown in Figure 1, seasonal changes of up to 5 ppbv in the mean surface O<sub>3</sub>  
276 concentration are observed during boreal summers, mainly in coastal regions and  
277 remote oceans. Surface O<sub>3</sub> changes in response to positive and negative SST anomalies  
278 generally exhibit a consistent spatial pattern but are opposite in sign, suggesting robust  
279 relationships between surface O<sub>3</sub> levels and SST anomalies (Figure 1). An increase in  
280 summertime SST over a specific ocean basin tends to increase the surface O<sub>3</sub>  
281 concentration over the upwind regions but reduce this concentration over downwind  
282 continents. For instance, a 1 °C warming over the North Pacific leads to a widespread  
283 decrease in surface O<sub>3</sub> over the North Pacific, North America and the North Atlantic of  
284 approximately 1 ppbv (Table S1) but may enhance the surface O<sub>3</sub> by nearly 3 ppbv over  
285 South China. Similarly, the SST warming over the North Atlantic decrease the surface  
286 O<sub>3</sub> levels by 1~2 ppbv over the North Atlantic and Europe but increase (~1 ppbv) that  
287 over North America and the North Pacific. For the North Indian Ocean, positive SST  
288 anomalies tend to increase the surface O<sub>3</sub> over the Indian Ocean and Africa but decrease  
289 the surface O<sub>3</sub> over South and East Asia (Figure 1). During the boreal winter, a  
290 widespread decrease in surface O<sub>3</sub> associated with the warming of different oceans is  
291 observed. Significant changes (e.g., up to 5 ppbv) mainly occur over remote ocean areas.  
292 Over populated continents, the response of the surface O<sub>3</sub> to basin-scale SST changes  
293 is typically insignificant. Details are shown in Figure S2 in the supplementary material.

294

295 Our simulations reveal that different oceans can exert distinct region-specific effects on  
296 the O<sub>3</sub> distribution. The effects of three individual warming/cooling cases (i.e., Pacific-  
297 W, Atlantic-W and Indian-W/Pacific-C, Atlantic-C and Indian-C) on surface O<sub>3</sub>  
298 distributions are further summed up to compare with the combined warming/cooling  
299 cases(i.e., ALL-W/ALL-C). The responses of surface O<sub>3</sub> to a hemispheric SST anomaly

300 generally resemble the sum of responses to individual regional SST changes (see  
301 Figures S3 and S4 in the supplementary material). This indicates that the effect of a  
302 generalized SST warming on surface O<sub>3</sub> can be decomposed into individual regional  
303 SST forcings. We now analyze the processes that impact the dependence of SST on the  
304 O<sub>3</sub> distribution using simulations that increase the SST.

#### 305 **4. Mechanism of SST-induced surface O<sub>3</sub> changes**

##### 306 **4.1 Process-level response to SST changes**

307 In this study, IPR analysis is used to evaluate the contribution of different  
308 physicochemical processes to O<sub>3</sub> evolution. The SST-induced, process-level O<sub>3</sub> changes  
309 are spatially averaged over four populated continental regions (i.e., NA, EU, EA and  
310 SA, Figure 2) and three ocean basins (i.e., the North Pacific, North Atlantic and North  
311 Indian Oceans, Figure S5). In most cases, VDIF and DRYD are the key processes  
312 controlling the O<sub>3</sub> variation. The downward transport of O<sub>3</sub> through diffusion (VDIF)  
313 is an important source of surface O<sub>3</sub>, while DRYD acts as a sink. Both processes are  
314 simultaneously determined by the strength of turbulence. Here, we define a new term  
315 TURB as the sum of DRYD and VDIF, which can capture the overall effect of  
316 turbulence changes on surface O<sub>3</sub> concentrations. In addition, we merge SHAL and  
317 DEEP as CONV to represent the total contribution of convective transport to surface  
318 O<sub>3</sub> (Figures 2 and S5). More detailed IPR results are shown in Figures S6 and S7 in the  
319 supplementary material.

320

321 In the “Pacific-W” case, a 1 °C SST warming over the North Pacific increases VDIF  
322 over eastern China in JJA (Figure S8), which is insignificant if averaged over the whole  
323 East Asia region. Meanwhile, this Pacific warming considerably reduces VDIF over  
324 North America (Figure S6). The corresponding decrease in TURB over North America  
325 mainly determines the surface O<sub>3</sub> reduction in JJA and SON, while the reduction in  
326 CONV exerts an additional negative impact (Figure 2). In the “Atlantic-W” case,  
327 increases in VDIF are also observed over the upwind regions (i.e., North America) in  
328 JJA. However, these increases are accompanied by commensurate decreases in DRYD,

329 resulting in an insignificant overall change in TURB (Figure 2). Therefore, the increase  
330 in CHEM is mainly responsible for the surface O<sub>3</sub> increase over North America in JJA.  
331 TURB is more relatively important over Europe (only in JJA and SON), leading to  
332 reduced surface O<sub>3</sub> abundance. In the “Indian-W” case, both CHEM and CONV are  
333 reduced over South Asia in JJA, leading to overall reductions in surface O<sub>3</sub> over the  
334 Indian subcontinent (Figure 2). The IPR analysis over the ocean basins shows that the  
335 warming of the North Pacific or North Atlantic induces reductions in VDIF and CHEM,  
336 which are responsible for the significant decrease in surface O<sub>3</sub> above these regions in  
337 JJA (Figure S7). The North Indian Ocean warming, on the other hand, enhances DEEP  
338 and VDIF, leading to a local increase in surface O<sub>3</sub> in JJA.

339

340 The IPR analysis indicates that, in general, an SST increase in the North Pacific or  
341 North Atlantic is more likely to enhance the vertical diffusion of O<sub>3</sub> over upwind  
342 regions (i.e., East Asia or North America, respectively) but suppress this diffusion over  
343 the ocean basin as well as downwind continents in JJA (Figure S8). These opposite  
344 changes in VDIF over upwind and downwind regions lead to distinct surface O<sub>3</sub>  
345 responses. Changes in CHEM enhance surface O<sub>3</sub> formation in most cases. An  
346 exception is in South Asia, where CHEM and DEEP dominate the reduction in surface  
347 O<sub>3</sub> over the region in JJA associated with the North Indian Ocean warming. In the  
348 following subsections, the mechanisms of the SST-O<sub>3</sub> relationship for the four polluted  
349 continents are further explored. Here we focus on boreal summers since the surface O<sub>3</sub>  
350 response to SST changes is more robust during this period than other seasons.

351

## 352 **4.2 Response of photochemical O<sub>3</sub> production to SST increases**

353 Changes in the net production rate (i.e., chemical production rate minus loss rate) of O<sub>3</sub>  
354 at the surface in JJA associated with basin-scale SST increases are shown in Figure 3.  
355 The peak changes are mainly confined to regions where O<sub>3</sub> precursors are abundant  
356 (e.g., South and East Asia and North America). For example, a warmer North Pacific  
357 SST exerts a positive (negative) impact on net O<sub>3</sub> production in the northern (southern)

358 regions of East Asia. Similarly, the warming of the North Atlantic promotes a dipole  
359 impact on the surface O<sub>3</sub> production over North America, while the warming of the  
360 North Indian Ocean significantly decreases the net O<sub>3</sub> production rate over South Asia.

361

362 As emissions are fixed in all simulations, the change in net O<sub>3</sub> production is driven by  
363 SST induced meteorological changes (e.g., air temperature, air humidity, and solar  
364 radiation). An increase in SST of 1 °C in any ocean basin leads to a widespread  
365 enhancement of the surface air temperature (i.e., the air temperature at 2 m) over most  
366 continental areas (Figure 4). An exception is the North Indian Ocean, where an increase  
367 in SST tends to cool the Indian subcontinent by 1-2 °C. This temperature decrease is  
368 not only limited to the surface but also spreads to 600 hPa (Figure S9). Associated with  
369 this temperature decrease is a remarkable reduction in the solar radiation received at the  
370 surface (more than 15 W/m<sup>2</sup>, Figure S10). Previous studies have indicated that moist  
371 convection is more sensitive to the SST changes in the tropical oceans than in mid- or  
372 high- latitude oceans (Lau and Nath, 1994; Lau et al., 1997; Hartmann, 2015). The SST  
373 increase over the North Indian Ocean tends to strengthen the moist convection that  
374 eventually facilitates cloud formation in the upper troposphere (Roxy et al., 2015; Xi et  
375 al., 2015; Chaudhari et al., 2016). The latent heat released from convective activities  
376 significantly warms the air temperature over the upper troposphere (Sabeerali et al.,  
377 2012; Xi et al., 2015). Meanwhile, the corresponding increase in cloud cover reduces  
378 the solar radiation reaching the surface of the Indian subcontinent and thus the air  
379 temperature of lower troposphere in that region. These processes lead to opposite air  
380 temperature changes between upper and lower troposphere over South Asia in response  
381 to the North Indian warming (as shown in Figure S9), which may further suppress the  
382 development of deep convection over the Indian subcontinent.

383

384 Previous studies have indicated that air temperature positively affects both O<sub>3</sub>  
385 production and destruction rates (Zeng et al., 2008; Pusede et al., 2015). As shown in  
386 Figure S11, changes in the net O<sub>3</sub> production rate are mainly dominated by O<sub>3</sub>  
387 production over continents but by O<sub>3</sub> destruction over oceans. An increase in SST leads

388 to a widespread enhancement of the air temperature, resulting in a positive change in  
389 the net O<sub>3</sub> production over most continental regions (Figure 3). However, a warmer SST  
390 also increases the air humidity (Figure S12), which enhances O<sub>3</sub> destruction over most  
391 coastal and oceanic areas. In addition, over South Asia, a warming of the North Indian  
392 Ocean decreases solar radiation and air temperature, and simultaneously increases air  
393 humidity, which jointly exert negative effects on O<sub>3</sub> production in that region.

394

### 395 **4.3 Response of physical O<sub>3</sub> transport to SST increases**

396 In Section 4.1, our IPR analysis highlights multiple physical processes (i.e., vertical  
397 diffusion, convection and advection) that are important in modulating surface O<sub>3</sub>  
398 concentrations. However, the role and relative importance of each process exhibit large  
399 spatial heterogeneity. In this section, we explore the key factors controlling physical O<sub>3</sub>  
400 transport in response to basin-scale SST changes.

401

402 The changes in the surface pressure and wind pattern induced by a basin-wide SST  
403 increase are shown in Figure 5. Generally, a warming of any ocean basin will lead to a  
404 low-pressure anomaly centered to its west at low-latitudes, which is caused by SST-  
405 induced convective activity. Additionally, the warming of the Indian Ocean induces an  
406 anticyclonic anomaly over the subtropical western Pacific, which has been documented  
407 in previous studies (Yang et al., 2007; Li et al., 2008). As shown in Figure 6, the surface  
408 pressure reduction induced by SST warming in any ocean basin is closely associated  
409 with enhanced upward motions, suggesting a substantial enhancement in deep  
410 convection over tropical oceans. Previous studies have identified an SST threshold  
411 (approximately 26°–28°C) to generating deep convection (Graham and Barnett, 1987;  
412 Johnson and Xie, 2010). Therefore, the sensitivity of deep convection to an SST  
413 anomaly is strongly dependent on the distribution of base SST. The enhanced upward  
414 motion in response to a uniform increase in basin-scale SST mainly occurs over regions  
415 with high climatological SST (Figure 6). Regions with a low climatological SST have  
416 little effects on the vertical movement of air masses.

417

418 Strengthened deep convection will trigger large-scale subsidence over nearby regions  
419 through the modulation of large-scale circulation patterns, which may suppress  
420 convective transport (Lau et al., 1997; Roxy et al., 2015; Ueda et al., 2015). This effect  
421 is verified by the decreases in upward velocity at 500 hPa. As depicted in Figure 6,  
422 significant decreases in upward velocity occur over regions adjacent to the strengthened  
423 deep convection. Similar effects are also observed over higher latitudes or remote  
424 oceans (Figure S13). Meanwhile, the air temperature increase in response to regional  
425 SST warming is more significant above the lower troposphere, which leads to a  
426 decrease in the vertical temperature gradient (Figure S9). These factors tend to restrain  
427 the vertical exchange of air pollutants at mid-latitudes, which facilitates surface O<sub>3</sub>  
428 accumulation over polluted continental regions in JJA but may weaken the intrusion of  
429 O<sub>3</sub> from the upper troposphere to the surface in most unpolluted areas. This process  
430 helps to explain the widespread decrease in surface O<sub>3</sub> over unpolluted regions  
431 associated with an SST increase, as described in Section 3, and can be further verified  
432 by the wide-spread reduction in VDIF shown in Figure S8.

433

434 The surface pressure anomalies induced by SST changes can play a dominant role in  
435 modulating surface O<sub>3</sub> transport at specific locations. For example, the low-pressure  
436 anomaly centered over the subtropical northwestern Pacific in the “Pacific-W” case  
437 causes the convergence of wind in the lower troposphere (Figure 5a). Consequently,  
438 surface O<sub>3</sub> pollution is enhanced in southern China due to an increase in O<sub>3</sub> transport  
439 from more polluted northern China (Figure 7a). The vertical distribution of the  
440 corresponding O<sub>3</sub> changes also shows that the increase in O<sub>3</sub> over southern China occurs  
441 below 700hPa, accompanied by noticeable decreases above 700hPa as well as over  
442 nearby northern China (Figure 7d). The IPR analysis also indicates that the increases in  
443 advective transport and downward turbulent transport are mainly responsible for the  
444 surface O<sub>3</sub> increase in southern China.

445

446 In the “Atlantic-W” case, the SST warming-induced surface pressure anomalies lead to

447 substantial O<sub>3</sub> redistribution, especially over the North Atlantic Ocean (Figure 7b). For  
448 North America, the changes in horizontal O<sub>3</sub> fluxes have no significant effect on the O<sub>3</sub>  
449 concentration increase. In addition, O<sub>3</sub> changes are observed to be larger in the upper  
450 troposphere than at the surface (Figure 7e). As demonstrated in Section 4.1, the  
451 response of lower-altitude O<sub>3</sub> over North America to the North Atlantic warming is  
452 mainly caused by enhanced chemical production, rather than physical transport.

453

454 The North Indian SST warming leads to a low-pressure anomaly centered over the  
455 Arabian Sea (Figure 5c). The warming of the North Indian Ocean strengthens the  
456 upward motion of air at low-latitudes and further induces a convergence of highly  
457 polluted air over the Indian Ocean. The effects of this process on O<sub>3</sub> concentrations are  
458 observed to be more significant in the upper troposphere (Figure 7f). According to the  
459 IPR analysis, the surface O<sub>3</sub> increase over the Indian Ocean is mainly caused by the  
460 enhanced vertical transport of O<sub>3</sub> to the surface through deep convection and vertical  
461 diffusion processes (Figure S7). However, over the nearby Indian subcontinent, the  
462 suppressed convection tends to decrease surface O<sub>3</sub> in that region (Figure 2).

463

## 464 **5. Implications for O<sub>3</sub> long-range transport**

465 The above findings indicate that, in general, a basin-scale SST increase in the Northern  
466 Hemisphere is more likely to enhance atmospheric stability at mid-latitudes, which may  
467 suppress air pollutants from lofting to the free troposphere. This process potentially has  
468 large effects on O<sub>3</sub> intercontinental transport. Following previous work (e.g., Doherty  
469 et al., 2013; Fang et al., 2011), we use passive CO-like tracers to demonstrate the  
470 potential effect of regional SST changes on long-range O<sub>3</sub> transport. A warming of  
471 North Pacific SSTs by 1°C tends to increase the East Asian CO tracer concentrations  
472 by nearly 6% at the surface (Figure 8b), which is accompanied by a significant  
473 reduction (~4%) in eastward transport to North America. Similarly, for the North  
474 American tracer, a warming of North Atlantic SSTs by 1°C increases (~1%) the  
475 concentrations in North America but decreases (3-4 %) the concentrations over

476 downwind Europe (Figure 8d). The response of the South Asian CO tracer to North  
477 Indian Ocean warming also shows a decreasing tendency over downwind regions, but  
478 the patterns are more complicated over the source region in this case (Figure 8e).  
479 Because the CO-like tracers added in the simulation have a fixed decay lifetime, their  
480 concentration changes are completely caused by the SST-induced transport anomalies.  
481 The decrease in CO tracer concentrations over downwind regions suggests that the  
482 warming of basin-scale SST tends to suppress the long-range transport of air pollutants.  
483 Additionally, in the “Pacific-W” case, changes in the East Asian CO tracer (Figure 8a)  
484 generally resemble the changes in surface O<sub>3</sub> over East Asia (Figure 7a), indicating the  
485 dominant effect of physical transport on the O<sub>3</sub> distribution over East Asia. Regarding  
486 the North American CO tracer in response to the North Atlantic warming or the South  
487 Asian CO tracer in response to the North Indian Ocean warming, their concentration  
488 changes are spatially inconsistent with those of O<sub>3</sub> (see Figures 7 and 8). This further  
489 indicates the distinct roles that different basin-scale SSTs play in nearby air quality.

490

491 Further investigations of zonal wind suggest that an increase in SST over different  
492 oceans consistently decreases the westerly winds at lower mid-latitudes (25°N - 45 °N)  
493 in the Northern Hemisphere but increases these winds at higher latitudes (Figure 9). In  
494 general, increases in the geopotential height induced by basin-scale SST warming are  
495 more significant at mid-latitudes than at other latitudes, which is consistent with the air  
496 temperature changes. Consequently, the meridional geopotential height gradient is  
497 decreasing at lower latitudes but increasing at higher latitudes, leading to corresponding  
498 changes in the westerly winds. The latitude band at 25°N - 45 °N covers many polluted  
499 regions (i.e., North America and East Asia). A weakened westerly wind may reduce  
500 long-rang O<sub>3</sub> transport. As demonstrated in Section 4.3, the basin-scale SST increases  
501 also exert negative effects on the upward transport of air masses at mid-latitudes.  
502 Therefore, the decreases in CO tracer concentrations over downwind regions (Figure  
503 8a and 8c) can be explained by both suppressed vertical transport and weakened  
504 westerly winds. In the “Indian-W” case, the SST increase over North India leads to a  
505 low-pressure anomaly above the Arabian Sea due to the enhanced deep convection (as

506 discussed in Section 4.3). The corresponding anomalous cyclonic circulation may be  
507 responsible for the dipole of the South Asian CO tracer changes over the source region  
508 depicted in Figure 8e.

509

510 In addition, we also find a hemispheric-scale decrease in peroxyacetyl nitrate (PAN), a  
511 reservoir of O<sub>3</sub> precursors (NO<sub>x</sub> and HO<sub>x</sub>) that facilitates the long-range transport of  
512 O<sub>3</sub>, during the warming of different oceans (Figure S14). This decrease is likely caused  
513 by the increase in the thermal decomposition of PAN in response to the air temperature  
514 increase (Jacob and Winner, 2009; Doherty et al., 2013).

515

516 Thus, it is reasonable to infer that, in general, the increased thermal decomposition of  
517 PAN, the weakened mid-latitude westerlies, and the reduced vertical air transport may  
518 exert a joint reducing effect on the intercontinental transport of O<sub>3</sub> during basin-scale  
519 SST increases.

520

## 521 **6. Summary**

522 In this paper, we investigate the responses of surface O<sub>3</sub> to basin-scale SST anomalies  
523 in the Northern Hemisphere. The latest version of CESM (version 1.2.2) is used in our  
524 simulation, forced with climatological and stationary SST anomalies ( $\pm 1$  °C) in the  
525 North Pacific, North Atlantic and North Indian Oceans, respectively. The responses of  
526 surface O<sub>3</sub> associated with these SST changes are evaluated. Results of similar  
527 magnitude but opposite sign are observed for the SST warming versus cooling  
528 simulations for each ocean basin, suggesting robust connections between the SST  
529 anomalies and surface O<sub>3</sub> changes. The regionally and seasonally averaged surface O<sub>3</sub>  
530 changes over four continental regions (i.e., NA, EU, EA and SA) produce wide seasonal  
531 and regional variability (varying from 1 to 3 ppbv). The warming of the North Pacific  
532 leads to nearly 3 ppbv increases in the surface O<sub>3</sub> over southern China in summer, with  
533 corresponding decreases over North America (~1 ppbv). Similarly, the North Atlantic  
534 SST warming elevates the surface O<sub>3</sub> pollution over North America while reducing the

535 surface O<sub>3</sub> (nearly 1-2 ppbv) over Europe. Changes in the North Indian SST exert  
536 significant impacts (1-3 ppbv) over South and East Asia during the entire year.

537

538 Process analysis indicates that dry deposition and vertical diffusion are two major  
539 processes governing the surface O<sub>3</sub> balance. The increase in SST in different ocean  
540 basins tends to increase the contributions of vertical diffusion to surface O<sub>3</sub> over upwind  
541 regions while greatly restraining that over downwind continents. These processes  
542 generally lead to widespread decreases in surface O<sub>3</sub>, which are partially offset by  
543 increases in air temperature-dependent chemical production rates. Specifically, the  
544 chemical production changes are mainly responsible for the surface O<sub>3</sub> increases over  
545 North America in response to the North Atlantic SST warming but exert a negative  
546 effect on South Asia in response to the North Indian SST warming. Decreases in the  
547 convective transport of O<sub>3</sub> to the surface associated with North Indian warming are  
548 significant over South Asia and exert a negative impact on surface O<sub>3</sub> concentrations.  
549 Advective transport has a positive effect on surface O<sub>3</sub> in southern China in the “Pacific-  
550 W” case.

551

552 We further show that air temperature is an important factor controlling the surface O<sub>3</sub>  
553 responses to SST anomalies. Reductions in the surface O<sub>3</sub> chemical production in South  
554 Asia associated with North Indian SST warming can be explained by the corresponding  
555 SST-induced decreases in ground-level air temperature and solar radiation. Meanwhile,  
556 the widespread increase in air temperature associated with basin-scale SST warming is  
557 more likely to promote O<sub>3</sub> production over other highly polluted regions.

558

559 On the other hand, SST increases at low latitudes over different oceans enhance deep  
560 convection in summer, which promotes convergence at the surface, as well as upward  
561 motions at low latitudes. The corresponding surface pressure anomalies centered over  
562 the east coast of East Asia associated with the North Pacific warming and over the  
563 Arabian Sea associated with the North Indian warming tend to increase the surface O<sub>3</sub>  
564 above through exchanges with the surrounding highly polluted air. The basin-scale SST

565 increases in the Northern Hemisphere reduce the tropospheric temperature gradient at  
566 mid-latitudes that restrains vertical transport of O<sub>3</sub> over continents and weakens the  
567 westerlies at lower mid-latitudes. The response of the CO-tracer also suggests that these  
568 factors may jointly exert a negative effect on the intercontinental transport of O<sub>3</sub>.

569

570 This study highlights the sensitivity of O<sub>3</sub> evolution to basin-wide SST changes in the  
571 Northern Hemisphere and identifies the key chemical or dynamical factors that control  
572 this evolution. Idealized and spatially uniform SST anomalies are used to explore the  
573 general mechanisms governing SST-O<sub>3</sub> relationships. We find that the SST changes  
574 over tropical regions exert considerable impacts on surface O<sub>3</sub> levels. The increase in  
575 tropical SST over different ocean basins enhances deep convection, which further  
576 trigger large-scale subsidence over nearby and remote regions. These enhanced  
577 convective activities also tend to release more latent heat over the upper troposphere  
578 and significantly increases the air temperature there. These processes influence large-  
579 scale circulation patterns and lead to opposite surface O<sub>3</sub> responses over upwind and  
580 downwind regions related to a specific ocean basin. These finding provides valuable  
581 implications for the potential surface O<sub>3</sub> change in response to future warming or  
582 cooling of individual oceans.

583

584 Additionally, the sensitivity tests with 1°C SST warming and cooling superimposed  
585 onto all three ocean basins further show in general that the SST forcing on O<sub>3</sub>  
586 distribution is geographically additive. A number of studies have used the decomposed  
587 SST anomalies for different regions to identify their relevant roles in a particular  
588 climate response (e.g., Sutton and Hodson, 2005; Camargo et al., 2013; Ueda et al.,  
589 2015). A linear assumption that the influence of large-scale SST anomaly pattern on the  
590 atmosphere can be generally constructed by the linear combination of the influences of  
591 individual SST patches have been verified by previous studies, especially for the  
592 tropical regions where the signal-to-noise is higher (e.g., Fan et al., 2016; Seager and  
593 Henderson, 2016). Therefore, our study also helps to understand the roles of different  
594 ocean basins in the Northern Hemisphere played in modulating surface O<sub>3</sub> distributions

595 in a global-wide SST warming condition associated with climate change.

596

597 Overall, this study may guide the management of regional O<sub>3</sub> pollution by considering  
598 the influence of specific SST variability. However, cautions should be taken in  
599 interpreting our results in the real world since observed surface O<sub>3</sub> variabilities are  
600 induced by various factors including O<sub>3</sub> precursor emissions and atmospheric  
601 conditions. Realistic SST anomalies over different oceans are more complicate (usually  
602 not uniformly distributed) and often inter-correlated with each other (Fan et al., 2016).  
603 They may exert jointly effects on modulating surface O<sub>3</sub> distributions. To provide more  
604 precise understanding about the SST-O<sub>3</sub> relationship over a specific region, additional  
605 sensitivity tests regarding smaller patches of SST variability are necessary.

606

#### 607 **Acknowledgements**

608 This work was supported by funding from the National Natural Science Foundation of  
609 China under awards 41671491, 41571130010, and 41390240, National Key Research  
610 and Development Program of China 2016YFC0206202, and the 111 Project (B14001).  
611 This work was also supported in part by the National Science Foundation under grant  
612 CBET-1512429.

613

#### 614 **References:**

615 Auvray, M., and Bey, I.: Long - range transport to Europe: Seasonal variations and implications for  
616 the European ozone budget, *Journal of Geophysical Research: Atmospheres* (1984-2012), 110,  
617 2005.  
618 Barnes, E. A., and Fiore, A. M.: Surface ozone variability and the jet position: Implications for  
619 projecting future air quality, *Geophys Res Lett*, 40, 2839-2844, 2013.  
620 Bloomer, B. J., Stehr, J. W., Piety, C. A., Salawitch, R. J., and Dickerson, R. R.: Observed  
621 relationships of ozone air pollution with temperature and emissions, *Geophys Res Lett*, 36,  
622 2009.  
623 Brasseur, G., Hauglustaine, D., Walters, S., Rasch, P., Müller, J. F., Granier, C., and Tie, X.:  
624 MOZART, a global chemical transport model for ozone and related chemical tracers: 1. Model  
625 description, *Journal of Geophysical Research: Atmospheres*, 103, 28265-28289, 1998.  
626 Bretherton, C. S., and Park, S.: A new moist turbulence parameterization in the Community  
627 Atmosphere Model, *J Climate*, 22, 3422-3448, 2009.

628 Bronnimann, S., Luterbacher, J., Schmutz, C., Wanner, H., and Staehelin, J.: Variability of total  
629 ozone at Arosa, Switzerland, since 1931 related to atmospheric circulation indices, *Geophys*  
630 *Res Lett*, 27, 2213-2216, 2000.

631 Brown-Steiner, B., and Hess, P.: Asian influence on surface ozone in the United States: A  
632 comparison of chemistry, seasonality, and transport mechanisms, *J Geophys Res-Atmos*, 116,  
633 Artn D1730910.1029/2011jd015846, 2011.

634 Brown, J., and Bowman, C.: Integrated Science Assessment for Ozone and Related Photochemical  
635 Oxidants, EPA 600/R-10, 2013.

636 Camalier, L., Cox, W., and Dolwick, P.: The effects of meteorology on ozone in urban areas and  
637 their use in assessing ozone trends, *Atmos Environ*, 41, 7127-7137, 2007.

638 Camargo, S. J., Ting, M., and Kushnir, Y.: Influence of local and remote SST on North Atlantic  
639 tropical cyclone potential intensity, *Clim Dynam*, 40, 1515-1529, 2013.

640 Chaudhari, H. S., Pokhrel, S., Kulkarni, A., Hazra, A., and Saha, S. K.: Clouds–SST relationship  
641 and interannual variability modes of Indian summer monsoon in the context of clouds and  
642 SSTs: observational and modelling aspects, *Int J Climatol*, 36, 4723-4740, 2016.

643 Christoudias, T., Pozzer, A., and Lelieveld, J.: Influence of the North Atlantic Oscillation on air  
644 pollution transport, *Atmos Chem Phys*, 12, 869-877, 2012.

645 Chuwah, C., van Noije, T., van Vuuren, D. P., Stehfest, E., and Hazeleger, W.: Global impacts of  
646 surface ozone changes on crop yields and land use, *Atmos Environ*, 106, 11-23,  
647 10.1016/j.atmosenv.2015.01.062, 2015.

648 Conley, A. J., Garcia, R., Kinnison, D., Lamarque, J.-F., Marsh, D., Mills, M., Smith, A. K., Tilmes,  
649 S., Vitt, F., and Morrison, H.: Description of the NCAR community atmosphere model (CAM  
650 5.0), NCAR technical note, 2012.

651 Creilson, J., Fishman, J., and Wozniak, A.: Intercontinental transport of tropospheric ozone: a study  
652 of its seasonal variability across the North Atlantic utilizing tropospheric ozone residuals and  
653 its relationship to the North Atlantic Oscillation, *Atmos Chem Phys*, 3, 2053-2066, 2003.

654 Dentener, F., Kinne, S., Bond, T., Boucher, O., Cofala, J., Generoso, S., Ginoux, P., Gong, S.,  
655 Hoelzemann, J., and Ito, A.: Emissions of primary aerosol and precursor gases in the years  
656 2000 and 1750 prescribed data-sets for AeroCom, *Atmos Chem Phys*, 6, 4321-4344, 2006.

657 Deser, C., Wahl, S., and Bates, J. J.: The influence of sea surface temperature gradients on stratiform  
658 cloudiness along the equatorial front in the Pacific Ocean, *J Climate*, 6, 1172-1180, 1993.

659 Deser, C., Alexander, M. A., Xie, S.-P., and Phillips, A. S.: Sea surface temperature variability:  
660 Patterns and mechanisms, *Annual Review of Marine Science*, 2, 115-143, 2010.

661 Ding, Y., Carton, J. A., Chepurin, G. A., Stenchikov, G., Robock, A., Sentman, L. T., and Krasting,  
662 J. P.: Ocean response to volcanic eruptions in Coupled Model Intercomparison Project 5  
663 simulations, *Journal of Geophysical Research: Oceans*, 119, 5622-5637, 2014.

664 Doherty, R. M., Wild, O., Shindell, D. T., Zeng, G., MacKenzie, I. A., Collins, W. J., Fiore, A. M.,  
665 Stevenson, D. S., Dentener, F. J., Schultz, M. G., Hess, P., Derwent, R. G., and Keating, T. J.:  
666 Impacts of climate change on surface ozone and intercontinental ozone pollution: A multi-  
667 model study, *J Geophys Res-Atmos*, 118, 3744-3763, 10.1002/jgrd.50266, 2013.

668 Emmons, L., Walters, S., Hess, P., Lamarque, J.-F., Pfister, G., Fillmore, D., Granier, C., Guenther, A.,  
669 Kinnison, D., and Laepple, T.: Description and evaluation of the Model for Ozone and Related  
670 chemical Tracers, version 4 (MOZART-4), *Geoscientific Model Development*, 3, 43-67, 2010.

671 Fallmann, J., Lewis, H., Castillo, J., Arnold, A., and Ramsdale, S.: Impact of sea surface temperature

672 on stratiform cloud formation over the North Sea, *Geophys Res Lett*, 2017.

673 Fan, L., Shin, S.-I., Liu, Z., and Liu, Q.: Sensitivity of Asian Summer Monsoon precipitation to  
674 tropical sea surface temperature anomalies, *Clim Dynam*, 47, 2501-2514, 2016.

675 Fan, M., and Schneider, E. K.: Observed decadal North Atlantic tripole SST variability. Part I:  
676 weather noise forcing and coupled response, *J Atmos Sci*, 69, 35-50, 2012.

677 Fang, Y., Fiore, A. M., Horowitz, L. W., Gnanadesikan, A., Held, I., Chen, G., Vecchi, G., and Levy,  
678 H.: The impacts of changing transport and precipitation on pollutant distributions in a future  
679 climate, *Journal of Geophysical Research: Atmospheres*, 116, 2011.

680 Fehsenfeld, F., Daum, P., Leaitch, W., Trainer, M., Parrish, D., and Hübler, G.: Transport and  
681 processing of O<sub>3</sub> and O<sub>3</sub> precursors over the North Atlantic: An overview of the 1993 North  
682 Atlantic Regional Experiment (NARE) summer intensive, *Journal of Geophysical Research:*  
683 *Atmospheres*, 101, 28877-28891, 1996.

684 Fiore, A., Dentener, F., Wild, O., Cuvelier, C., Schultz, M., Hess, P., Textor, C., Schulz, M., Doherty,  
685 R., and Horowitz, L.: Multimodel estimates of intercontinental source - receptor relationships  
686 for ozone pollution, *Journal of Geophysical Research: Atmospheres (1984-2012)*, 114, 2009.

687 Frankignoul, C.: Sea surface temperature anomalies, planetary waves, and air - sea feedback in the  
688 middle latitudes, *Reviews of geophysics*, 23, 357-390, 1985.

689 Frankignoul, C., and Sennéchal, N.: Observed influence of North Pacific SST anomalies on the  
690 atmospheric circulation, *J Climate*, 20, 592-606, 2007.

691 Gettelman, A., Morrison, H., and Ghan, S. J.: A new two-moment bulk stratiform cloud  
692 microphysics scheme in the Community Atmosphere Model, version 3 (CAM3). Part II:  
693 Single-column and global results, *J Climate*, 21, 3660-3679, 2008.

694 Ghan, S. J., Liu, X., Easter, R. C., Zaveri, R., Rasch, P. J., Yoon, J.-H., and Eaton, B.: Toward a  
695 minimal representation of aerosols in climate models: Comparative decomposition of aerosol  
696 direct, semidirect, and indirect radiative forcing, *J Climate*, 25, 6461-6476, 2012.

697 Giorgi, F., and Chameides, W.: The rainout parameterization in a photochemical model, *Journal of*  
698 *Geophysical Research: Atmospheres*, 90, 7872-7880, 1985.

699 Glantz, M. H., Katz, R. W., and Nicholls, N.: Teleconnections linking worldwide climate anomalies,  
700 Cambridge University Press Cambridge, 1991.

701 Goswami, B., Madhusoodanan, M., Neema, C., and Sengupta, D.: A physical mechanism for North  
702 Atlantic SST influence on the Indian summer monsoon, *Geophys Res Lett*, 33, 2006.

703 Graham, N., and Barnett, T.: Sea surface temperature, surface wind divergence, and convection over  
704 tropical oceans, *Science*, 238, 657-659, 1987.

705 Grewe, V.: The origin of ozone, *Atmos Chem Phys*, 6, 1495-1511, 2006.

706 Guenther, R.: Isoprene and monoterpene emission rate variability: model evaluations and sensitivity  
707 analyses, *J Geophys Res*, 98, 1993.

708 Gulev, S. K., Latif, M., Keenlyside, N., Park, W., and Koltermann, K. P.: North Atlantic Ocean  
709 control on surface heat flux on multidecadal timescales, *Nature*, 499, 464-467, 2013.

710 Hartmann, D. L.: Pacific sea surface temperature and the winter of 2014, *Geophys Res Lett*, 42,  
711 1894-1902, 2015.

712 Hess, P., and Mahowald, N.: Interannual variability in hindcasts of atmospheric chemistry: the role  
713 of meteorology, *Atmos. Chem. Phys*, 9, 5261-5280, 2009.

714 Horowitz, L. W., Walters, S., Mauzerall, D. L., Emmons, L. K., Rasch, P. J., Granier, C., Tie, X.,  
715 Lamarque, J. F., Schultz, M. G., and Tyndall, G. S.: A global simulation of tropospheric ozone

716 and related tracers: Description and evaluation of MOZART, version 2, *Journal of*  
717 *Geophysical Research: Atmospheres* (1984–2012), 108, 2003.

718 Hsieh, W. C., Collins, W. D., Liu, Y., Chiang, J. C. H., Shie, C. L., Caldeira, K., and Cao, L.: Climate  
719 response due to carbonaceous aerosols and aerosol-induced SST effects in NCAR community  
720 atmospheric model CAM3.5, *Atmos Chem Phys*, 13, 7489-7510, DOI 10.5194/acp-13-7489-  
721 2013, 2013.

722 Hurrell, J. W., Hack, J. J., Shea, D., Caron, J. M., and Rosinski, J.: A new sea surface temperature  
723 and sea ice boundary dataset for the Community Atmosphere Model, *J Climate*, 21, 5145-  
724 5153, 2008.

725 IPCC: Climate Change 2013: the physical science basis, in: Contribution of Working Group I to the  
726 Fifth Assessment Report of the Intergovernmental Panel on Climate Change, edited by:  
727 Stocker, T. F., Qin, D., Plattner, G.-K., Tignor, M., Allen, S. K., Boschung, J., Nauels, A., Xia,  
728 Y., Bex, V. and Midgley, P. M., Cambridge University Press, Cambridge, United Kingdom  
729 and New York, NY, USA, 1535 pp., 2013.

730 Jacob, D.: Introduction to atmospheric chemistry, Princeton University Press, 1999.

731 Jacob, D. J., and Winner, D. A.: Effect of climate change on air quality, *Atmos Environ*, 43, 51-63,  
732 2009.

733 Jiang, Z., Miyazaki, K., Worden, J. R., Liu, J. J., Jones, D., and Henze, D. K.: Impacts of  
734 anthropogenic and natural sources on free tropospheric ozone over the Middle East, *Atmos*  
735 *Chem Phys*, 16, 6537-6546, 2016.

736 Johnson, C., Collins, W., Stevenson, D., and Derwent, R.: Relative roles of climate and emissions  
737 changes on future tropospheric oxidant concentrations, *Journal of Geophysical Research:*  
738 *Atmospheres* (1984–2012), 104, 18631-18645, 1999.

739 Johnson, N. C., and Xie, S.-P.: Changes in the sea surface temperature threshold for tropical  
740 convection, *Nat Geosci*, 3, 842-845, 2010.

741 Knowland, K., Doherty, R., and Hodges, K. I.: The effects of springtime mid-latitude storms on  
742 trace gas composition determined from the MACC reanalysis, *Atmos Chem Phys*, 15, 3605-  
743 3628, 2015.

744 Kushnir, Y.: Interdecadal variations in North Atlantic sea surface temperature and associated  
745 atmospheric conditions, *J Climate*, 7, 141-157, 1994.

746 Kushnir, Y., Robinson, W., Bladé, I., Hall, N., Peng, S., and Sutton, R.: Atmospheric GCM response  
747 to extratropical SST anomalies: Synthesis and evaluation\*, *J Climate*, 15, 2233-2256, 2002.

748 Lamarque, J.-F., Bond, T. C., Eyring, V., Granier, C., Heil, A., Klimont, Z., Lee, D., Liousse, C.,  
749 Mieville, A., and Owen, B.: Historical (1850–2000) gridded anthropogenic and biomass  
750 burning emissions of reactive gases and aerosols: methodology and application, *Atmos Chem*  
751 *Phys*, 10, 7017-7039, 2010.

752 Lamarque, J., Emmons, L., Hess, P., Kinnison, D. E., Tilmes, S., Vitt, F., Heald, C., Holland, E. A.,  
753 Lauritzen, P., and Neu, J.: CAM-chem: Description and evaluation of interactive atmospheric  
754 chemistry in the Community Earth System Model, *Geosci. Model Dev*, 5, 369-411, 2012.

755 Lamarque, J. F., and Hess, P. G.: Arctic Oscillation modulation of the Northern Hemisphere spring  
756 tropospheric ozone, *Geophys Res Lett*, 31, 2004.

757 Lau, K., Wu, H., and Bony, S.: The role of large-scale atmospheric circulation in the relationship  
758 between tropical convection and sea surface temperature, *J Climate*, 10, 381-392, 1997.

759 Lau, N.-C., and Nath, M. J.: A modeling study of the relative roles of tropical and extratropical SST

760 anomalies in the variability of the global atmosphere-ocean system, *J Climate*, 7, 1184-1207,  
761 1994.

762 Lau, N.-C.: Interactions between global SST anomalies and the midlatitude atmospheric circulation,  
763 *B Am Meteorol Soc*, 78, 21-33, 1997.

764 Li, L., Chen, C., Huang, C., Huang, H., Zhang, G., Wang, Y., Wang, H., Lou, S., Qiao, L., and Zhou,  
765 M.: Process analysis of regional ozone formation over the Yangtze River Delta, China using  
766 the Community Multi-scale Air Quality modeling system, *Atmos Chem Phys*, 12, 10971-  
767 10987, 2012.

768 Li, S., Lu, J., Huang, G., and Hu, K.: Tropical Indian Ocean basin warming and East Asian summer  
769 monsoon: A multiple AGCM study, *J Climate*, 21, 6080-6088, 2008.

770 Lin, M., Fiore, A. M., Horowitz, L. W., Cooper, O. R., Naik, V., Holloway, J., Johnson, B. J.,  
771 Middlebrook, A. M., Oltmans, S. J., and Pollack, I. B.: Transport of Asian ozone pollution  
772 into surface air over the western United States in spring, *Journal of Geophysical Research:*  
773 *Atmospheres*, 117, 2012a.

774 Lin, M., Horowitz, L. W., Oltmans, S. J., Fiore, A. M., and Fan, S.: Tropospheric ozone trends at  
775 Mauna Loa Observatory tied to decadal climate variability, *Nat Geosci*, 7, 136-143, 2014.

776 Lin, M., Fiore, A. M., Horowitz, L. W., Langford, A. O., Oltmans, S. J., Tarasick, D., and Rieder, H.  
777 E.: Climate variability modulates western US ozone air quality in spring via deep stratospheric  
778 intrusions, *Nat Commun*, 6, 2015.

779 Lin, M. Y., Fiore, A. M., Cooper, O. R., Horowitz, L. W., Langford, A. O., Levy, H., Johnson, B. J.,  
780 Naik, V., Oltmans, S. J., and Senff, C. J.: Springtime high surface ozone events over the  
781 western United States: Quantifying the role of stratospheric intrusions, *J Geophys Res-Atmos*,  
782 117, Artn D00v2210.1029/2012jd018151, 2012b.

783 Liu, J., Mauzerall, D. L., and Horowitz, L. W.: Analysis of seasonal and interannual variability in  
784 transpacific transport, *Journal of Geophysical Research: Atmospheres*, 110, 2005.

785 Liu, X., and Ghan, S.: A modal aerosol model implementation in the community atmosphere model,  
786 version 5 (CAM5), *J. Atmos. Sci*, 2010.

787 Mantua, N. J., and Hare, S. R.: The Pacific decadal oscillation, *J Oceanogr*, 58, 35-44, 2002.

788 Meehl, G. A., Teng, H., Maher, N., and England, M. H.: Effects of the Mount Pinatubo eruption on  
789 decadal climate prediction skill of Pacific sea surface temperatures, *Geophys Res Lett*, 42,  
790 2015.

791 Morrison, H., and Gettelman, A.: A new two-moment bulk stratiform cloud microphysics scheme  
792 in the Community Atmosphere Model, version 3 (CAM3). Part I: Description and numerical  
793 tests, *J Climate*, 21, 3642-3659, 2008.

794 Ordóñez, C., Mathis, H., Furger, M., Henne, S., Hüglin, C., Staehelin, J., and Prévôt, A.: Changes  
795 of daily surface ozone maxima in Switzerland in all seasons from 1992 to 2002 and discussion  
796 of summer 2003, *Atmos Chem Phys*, 5, 1187-1203, 2005.

797 Park, S., and Bretherton, C. S.: The University of Washington shallow convection and moist  
798 turbulence schemes and their impact on climate simulations with the Community Atmosphere  
799 Model, *J Climate*, 22, 3449-3469, 2009.

800 Parrish, D. D., Holloway, J. S., Trainer, M., Murphy, P. C., Fehsenfeld, F. C., and Forbes, G. L.:  
801 Export of North American ozone pollution to the north Atlantic Ocean, *Science*, 259, 1436-  
802 1439, 1993.

803 Pausata, F. S., Pozzoli, L., Vignati, E., and Dentener, F. J.: North Atlantic Oscillation and

804 tropospheric ozone variability in Europe: model analysis and measurements intercomparison,  
805 *Atmos Chem Phys*, 12, 6357-6376, 2012.

806 Peñuelas, J., and Llusà, J.: The complexity of factors driving volatile organic compound emissions  
807 by plants, *Biologia Plantarum*, 44, 481-487, 2001.

808 Philander, S. G. H.: El Niño southern oscillation phenomena, *Nature*, 302, 295-301, 1983.

809 Price, C., Penner, J., and Prather, M.: NO<sub>x</sub> from lightning: 1. Global distribution based on lightning  
810 physics, *Journal of Geophysical Research: Atmospheres* (1984–2012), 102, 5929-5941, 1997.

811 Pusede, S. E., Steiner, A. L., and Cohen, R. C.: Temperature and Recent Trends in the Chemistry of  
812 Continental Surface Ozone, *Chem Rev*, 115, 3898-3918, 10.1021/cr5006815, 2015.

813 Rasmussen, D. J., Fiore, A. M., Naik, V., Horowitz, L. W., McGinnis, S. J., and Schultz, M. G.:  
814 Surface ozone-temperature relationships in the eastern US: A monthly climatology for  
815 evaluating chemistry-climate models, *Atmos Environ*, 47, 142-153,  
816 10.1016/j.atmosenv.2011.11.021, 2012.

817 Raymond, D., and Blyth, A.: Extension of the stochastic mixing model to cumulonimbus clouds, *J*  
818 *Atmos Sci*, 49, 1968-1983, 1992.

819 Raymond, D. J., and Blyth, A. M.: A stochastic mixing model for nonprecipitating cumulus clouds,  
820 *J Atmos Sci*, 43, 2708-2718, 1986.

821 Richter, J. H., and Rasch, P. J.: Effects of convective momentum transport on the atmospheric  
822 circulation in the Community Atmosphere Model, version 3, *J Climate*, 21, 1487-1499, 2008.

823 Rotstayn, L. D., and Lohmann, U.: Tropical rainfall trends and the indirect aerosol effect, *J Climate*,  
824 15, 2103-2116, 2002. Roxy, M. K., Ritika, K., Terray, P., Murtugudde, R., Ashok, K., and  
825 Goswami, B.: Drying of Indian subcontinent by rapid Indian Ocean warming and a weakening  
826 land-sea thermal gradient, *Nat Commun*, 6, 2015.

827 Sabeerali, C., Rao, S. A., Ajayamohan, R., and Murtugudde, R.: On the relationship between Indian  
828 summer monsoon withdrawal and Indo-Pacific SST anomalies before and after 1976/1977  
829 climate shift, *Clim Dynam*, 39, 841-859, 2012.

830 Saji, N., Goswami, B., Vinayachandran, P., and Yamagata, T.: A dipole mode in the tropical Indian  
831 Ocean, *Nature*, 401, 360-363, 1999.

832 Seager, R., and Henderson, N.: On the Role of Tropical Ocean Forcing of the Persistent North  
833 American West Coast Ridge of Winter 2013/14 a, *J Climate*, 29, 8027-8049, 2016.

834 Shindell, D., Chin, M., Dentener, F., Doherty, R., Faluvegi, G., Fiore, A. M., Hess, P., Koch, D.,  
835 MacKenzie, I., and Sanderson, M.: A multi-model assessment of pollution transport to the  
836 Arctic, *Atmos Chem Phys*, 8, 5353-5372, 2008.

837 Sillman, S., and Samson, P. J.: Impact of temperature on oxidant photochemistry in urban, polluted  
838 rural and remote environments, *Journal of Geophysical Research: Atmospheres*, 100, 11497-  
839 11508, 1995.

840 Simmonds, P., Derwent, R., Manning, A., and Spain, G.: Significant growth in surface ozone at  
841 Mace Head, Ireland, 1987–2003, *Atmos Environ*, 38, 4769-4778, 2004.

842 Simon, H., Reff, A., Wells, B., Xing, J., and Frank, N.: Ozone trends across the United States over  
843 a period of decreasing NO<sub>x</sub> and VOC emissions, *Environ Sci Technol*, 49, 186-195, 2014.

844 Small, R., Xie, S., O'Neill, L., Seo, H., Song, Q., Cornillon, P., Spall, M., and Minobe, S.: Air–sea  
845 interaction over ocean fronts and eddies, *Dynam Atmos Oceans*, 45, 274-319, 2008.

846 Sutton, R. T., and Hodson, D. L.: Atlantic Ocean forcing of North American and European summer  
847 climate, *Science*, 309, 115-118, 2005.

848 Sutton, R. T., and Hodson, D. L.: Climate response to basin-scale warming and cooling of the North  
849 Atlantic Ocean, *J Climate*, 20, 891-907, 2007.

850 Taboada, F. G., and Anadon, R.: Patterns of change in sea surface temperature in the North Atlantic  
851 during the last three decades: beyond mean trends, *Climatic Change*, 115, 419-431, 2012.

852 Tao, W., Liu, J., Ban-Weiss, G., Hauglustaine, D., Zhang, L., Zhang, Q., Cheng, Y., Yu, Y., and Tao,  
853 S.: Effects of urban land expansion on the regional meteorology and air quality of eastern  
854 China, *Atmos Chem Phys*, 15, 8597-8614, 2015.

855 Taschetto, A., Rodrigues, R., Meehl, G., McGregor, S., and England, M.: How sensitive are the  
856 Pacific–tropical North Atlantic teleconnections to the position and intensity of El Niño-related  
857 warming?, *Clim Dynam*, 46, 1841-1860, 2016.

858 Tie, X., Madronich, S., Walters, S., Edwards, D. P., Ginoux, P., Mahowald, N., Zhang, R., Lou, C.,  
859 and Brasseur, G.: Assessment of the global impact of aerosols on tropospheric oxidants,  
860 *Journal of Geophysical Research: Atmospheres*, 110, 2005.

861 Tilmes, S., Lamarque, J.-F., Emmons, L., Kinnison, D., Ma, P.-L., Liu, X., Ghan, S., Bardeen, C.,  
862 Arnold, S., and Deeter, M.: Description and evaluation of tropospheric chemistry and aerosols  
863 in the Community Earth System Model (CESM1. 2), *Geoscientific Model Development*  
864 *Discussions*, 7, 8875-8940, 2014.

865 Ueda, H., Kamae, Y., Hayasaki, M., Kitoh, A., Watanabe, S., Miki, Y., and Kumai, A.: Combined  
866 effects of recent Pacific cooling and Indian Ocean warming on the Asian monsoon, *Nat*  
867 *Commun*, 6, 2015.

868 Vingarzan, R.: A review of surface ozone background levels and trends, *Atmos Environ*, 38, 3431-  
869 3442, 2004.

870 Walmsley, J. L., and Wesely, M. L.: Modification of coded parametrizations of surface resistances  
871 to gaseous dry deposition, *Atmos Environ*, 30, 1181-1188, 1996.

872 Wang, B., Wu, R., and Fu, X.: Pacific-East Asian teleconnection: how does ENSO affect East Asian  
873 climate?, *J Climate*, 13, 1517-1536, 2000.

874 Wang, C., Deser, C., Yu, J.-Y., DiNezio, P., and Clement, A.: El Nino and southern oscillation  
875 (ENSO): a review, *Coral Reefs of the Eastern Pacific*, 3-19, 2012.

876 Wang, X., Zhang, Y., Hu, Y., Zhou, W., Lu, K., Zhong, L., Zeng, L., Shao, M., Hu, M., and Russell,  
877 A.: Process analysis and sensitivity study of regional ozone formation over the Pearl River  
878 Delta, China, during the PRIDE-PRD2004 campaign using the Community Multiscale Air  
879 Quality modeling system, *Atmos Chem Phys*, 10, 4423-4437, 2010.

880 Webster, P. J.: Mechanisms determining the atmospheric response to sea surface temperature  
881 anomalies, *J Atmos Sci*, 38, 554-571, 1981.

882 Wesely, M.: Parameterization of surface resistances to gaseous dry deposition in regional-scale  
883 numerical models, *Atmospheric Environment (1967)*, 23, 1293-1304, 1989.

884 Wesely, M., and Hicks, B.: A review of the current status of knowledge on dry deposition, *Atmos*  
885 *Environ*, 34, 2261-2282, 2000.

886 Wild, O., and Akimoto, H.: Intercontinental transport of ozone and its precursors in a three-  
887 dimensional global CTM, *Journal of Geophysical Research: Atmospheres*, 106, 27729-27744,  
888 2001.

889 World Health Organization: Review of evidence on health aspects of air pollution–REVIHAAP  
890 Project, World Health Organization, Copenhagen, Denmark, 2013.

891 Wu, L., and Liu, Z.: North Atlantic Decadal Variability: Air-Sea Coupling, Oceanic Memory, and

892 Potential Northern Hemisphere Resonance\*, *J Climate*, 18, 331-349, 2005.

893 Wu, R. G., and Kinter, J. L.: Shortwave radiation-SST relationship over the mid-latitude North  
894 Pacific during boreal summer in climate models, *Clim Dynam*, 36, 2251-2264, DOI  
895 10.1007/s00382-010-0775-5, 2011.

896 Wu, S., Mickley, L. J., Leibensperger, E. M., Jacob, D. J., Rind, D., and Streets, D. G.: Effects of  
897 2000–2050 global change on ozone air quality in the United States, *Journal of Geophysical*  
898 *Research: Atmospheres*, 113, 2008.

899 Xi, J., Zhou, L., Murtugudde, R., and Jiang, L.: Impacts of intraseasonal sst anomalies on  
900 precipitation during Indian summer monsoon, *J Climate*, 28, 4561-4575, 2015.

901 Yang, J., Liu, Q., Xie, S. P., Liu, Z., and Wu, L.: Impact of the Indian Ocean SST basin mode on the  
902 Asian summer monsoon, *Geophys Res Lett*, 34, 2007.

903 Zeng, G., Pyle, J., and Young, P.: Impact of climate change on tropospheric ozone and its global  
904 budgets, *Atmos Chem Phys*, 8, 369-387, 2008.

905 Zhang, G. J., and McFarlane, N. A.: Sensitivity of climate simulations to the parameterization of  
906 cumulus convection in the Canadian Climate Centre general circulation model, *Atmos Ocean*,  
907 33, 407-446, 1995.

908 Zhang, L., Jacob, D. J., Yue, X., Downey, N. V., Wood, D. A., and Blewitt, D.: Sources contributing  
909 to background surface ozone in the US Intermountain West, *Atmos Chem Phys*, 14, 5295-  
910 5309, 10.5194/acp-14-5295-2014, 2014.

911 Zhang, Y., and Wu, S.-Y.: Understanding of the Fate of Atmospheric Pollutants Using a Process  
912 Analysis Tool in a 3-D Regional Air Quality Model at a Fine Grid Scale, *Atmospheric and*  
913 *Climate Sciences*, 3, 18, 2013.

914

915

916

917

918

919

920

921

922

923

924

925

926

927

928

929

930

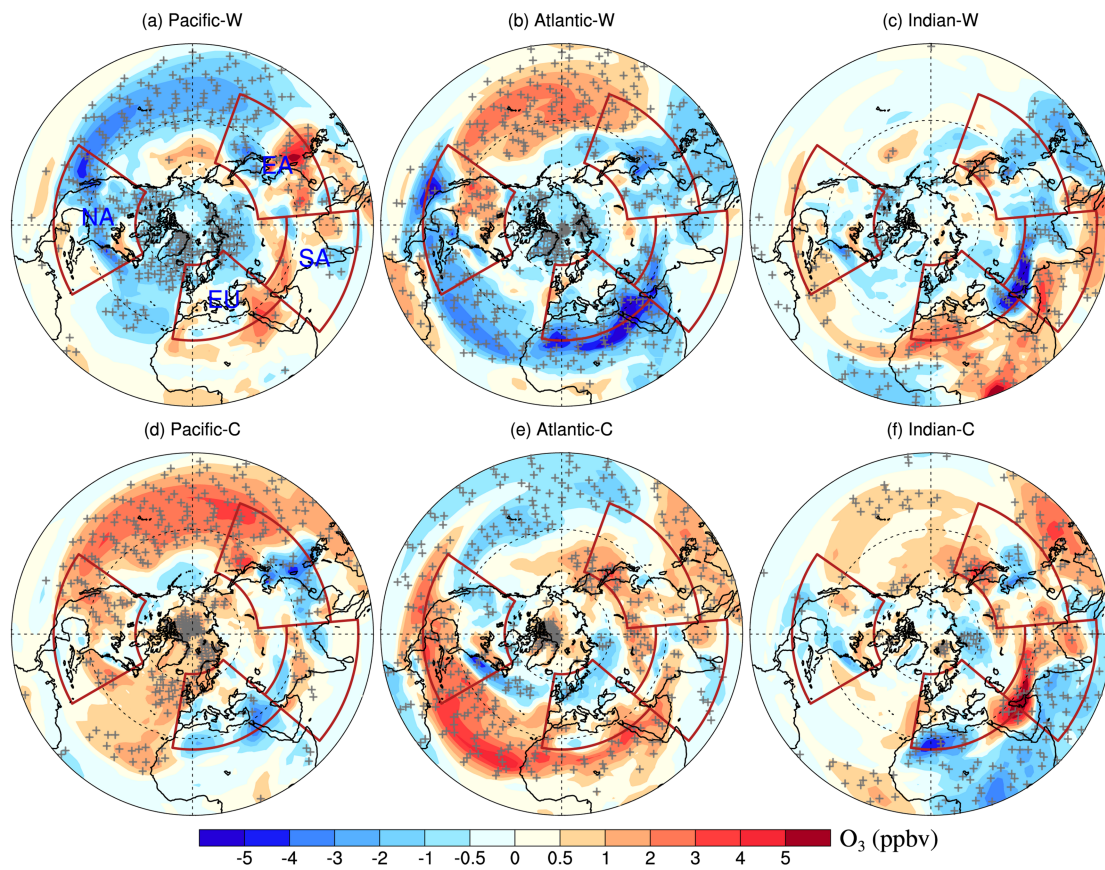
931

932 **Table 1.** Seasonally (i.e., DJF (December, January, February), MAM (March, April,  
 933 May), JJA (June, July, August) and SON (September, October, November)) and  
 934 regionally averaged (only land grid boxes are included) changes in surface O<sub>3</sub>  
 935 concentrations (ppbv) for basin-scale SST perturbation cases relative to the control  
 936 simulation. Positive (negative) changes that are significant at the 0.05 level evaluated  
 937 by Student's t-test are marked in red (blue).

Ozone (ppbv)		DJF	MAM	JJA	SON	
North Pacific	+1° C	North America	-0.27*	-0.42*	-0.92*	-1.03*
		Europe	-0.50*	-0.26	0.10	-0.29
		East Asia	-0.88*	-0.71*	0.20	0.17
		South Asia	-1.00*	0.30	0.43	0.43*
	-1° C	North America	0.00	0.57*	0.55*	0.82*
		Europe	0.19	0.15	-0.47*	0.47*
		East Asia	0.30	-0.17	-0.22	-0.67*
		South Asia	0.04	-0.24	0.03	-0.40
North Atlantic	+1° C	North America	0.03	0.49	0.50*	0.53*
		Europe	0.30*	0.06	-1.61*	-0.89*
		East Asia	-0.52*	-0.68*	-0.62*	-0.25
		South Asia	-0.20	-1.46*	-1.28*	-0.82*
	-1° C	North America	-0.07	-0.10	0.10	-0.17
		Europe	0.00	0.00	0.07	0.06
		East Asia	0.16	-0.08	0.80*	-0.60*
		South Asia	-0.20	-0.40	0.30	-0.10
North India	+1° C	North America	-0.25	-0.04	-0.16	-0.10
		Europe	-0.30	0.08	-0.12	0.19
		East Asia	-0.53*	-0.77*	-0.28	-1.78*
		South Asia	-1.00*	0.14	-1.67*	-2.75*
	-1° C	North America	0.04	0.17	0.04	0.25
		Europe	0.05	-0.07	-0.13	-0.24
		East Asia	-0.06	0.15	0.55*	0.33
		South Asia	-0.03	0.57	1.70*	1.31*

938 \*Significant at the 0.05 level from Student's t-test using 20 years of model results.

939



941

942 **Figure 1.** Changes in the summertime (June-August) surface O<sub>3</sub> concentrations (ppbv)

943 in the Northern Hemisphere induced by 1°C warming (top) and 1°C cooling (bottom)

944 in the North Pacific Ocean (left), North Atlantic Ocean (center), and North Indian

945 Ocean (right) relative to the CTRL. The four major regions of interest (i.e., NA (15°N–

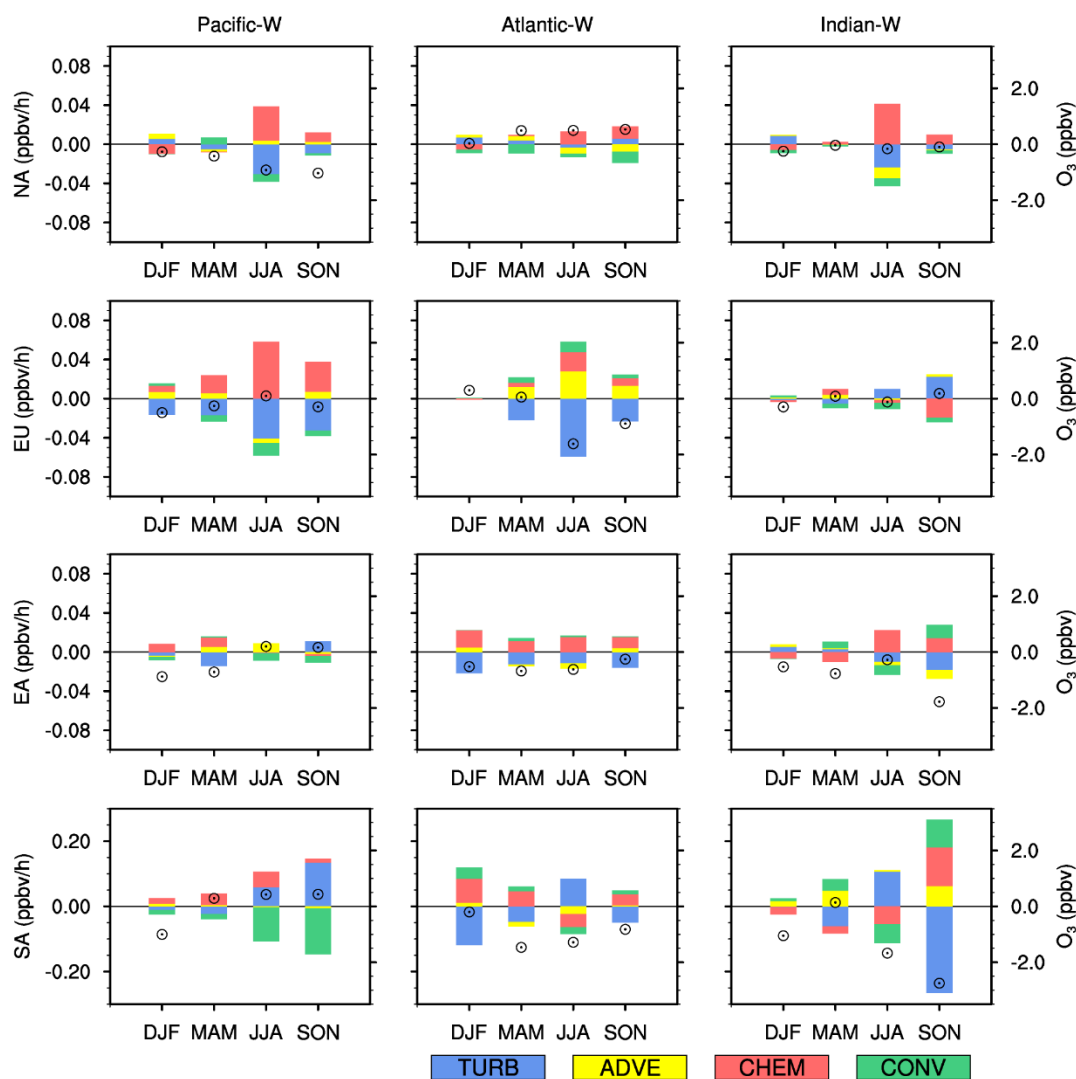
946 55°N; 60°W–125°W), EU (25°N–65°N; 10°W–50°E), EA (15°N–50°N; 95°E–160°E)

947 and SA (5°N–35°N; 50°E–95°E)) are marked with red polygons. The + symbols denote

948 areas where results are significant at the 0.05 level, evaluated by Student's t-test using

949 20 years of data.

950



951

952 **Figure 2.** Seasonally averaged changes in the IPR contributions (bars, ppbv/h, left scale)

953 and surface O<sub>3</sub> concentrations (hollow circles, ppbv, right scale) for Pacific-W (left),

954 Atlantic-W (middle) and Indian-W (right) relative to the CTRL. Values are regionally

955 averaged over NA (first row), EU (second row), EA (third row) and SA (last row).

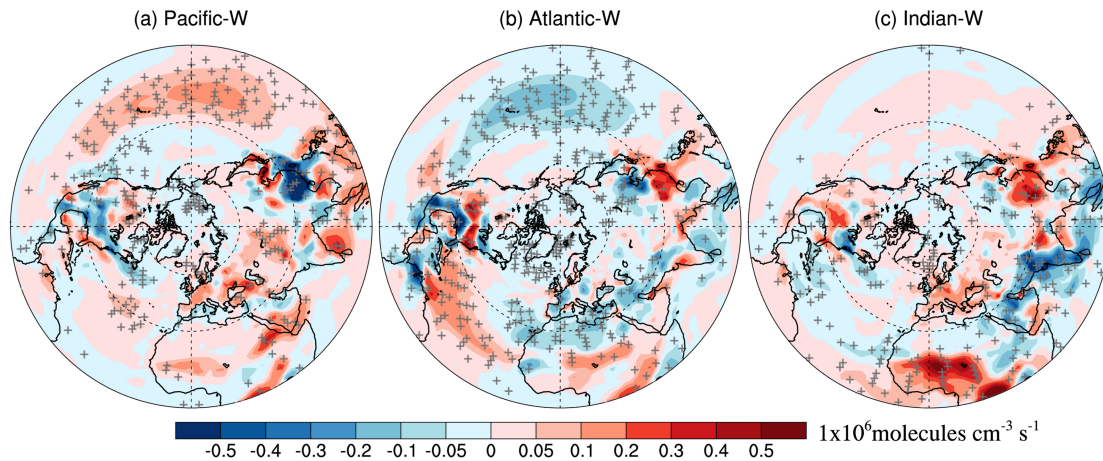
956 TURB is defined as the sum of VDIF and DRYD. CONV is the sum of DEEP and

957 SHAL. IPR contributions from the four processes (i.e., TURB, ADVE, CHEM and

958 CONV) are represented by different colors. A more detailed IPR result is shown in

959 Figure S6 in the supplementary material.

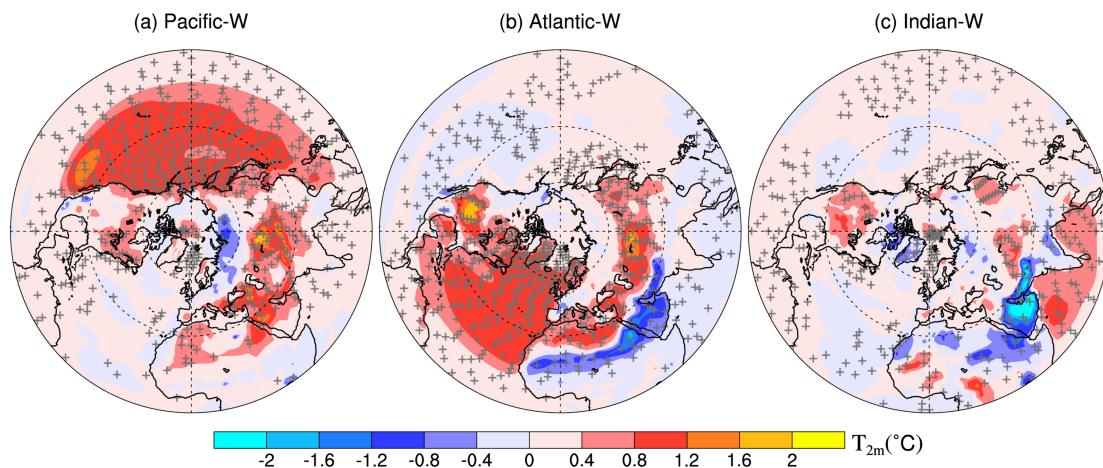
960



961

962 **Figure 3.** Perturbations of the surface net O<sub>3</sub> production rate ( $1 \times 10^6$  molecules cm<sup>-3</sup> s<sup>-1</sup>) for (a) Pacific-W, (b) Atlantic-W, and (c) Indian-W relative to the CTRL in the boreal summer. The + symbols denote areas where the results are significant at the 0.05 level, evaluated by Student's t-test using 20 years of data.

966

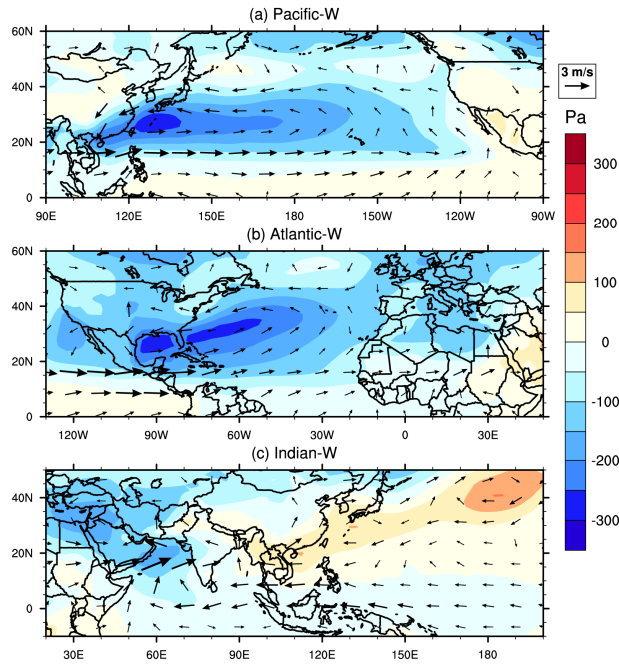


967

968 **Figure 4.** Changes in the surface air temperature (°C) for (a) Pacific-W, (b) Atlantic-W, and (c) Indian-W relative to CTRL in the Northern Hemisphere in the boreal summer. The + symbols denote areas where the results are significant at the 0.05 level, evaluated by Student's t-test using 20 years of data.

972

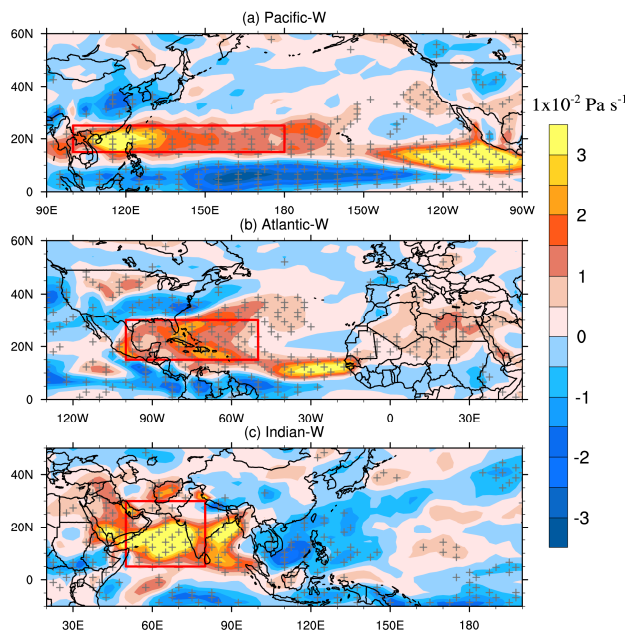
973



974

975 **Figure 5.** Changes in the surface pressure (color contours, Pa) and 850-hPa wind  
 976 (arrows,  $\text{m s}^{-1}$ ) for (a) Pacific-W, (b) Atlantic-W, and (c) Indian-W relative to the CTRL  
 977 in the boreal summer.

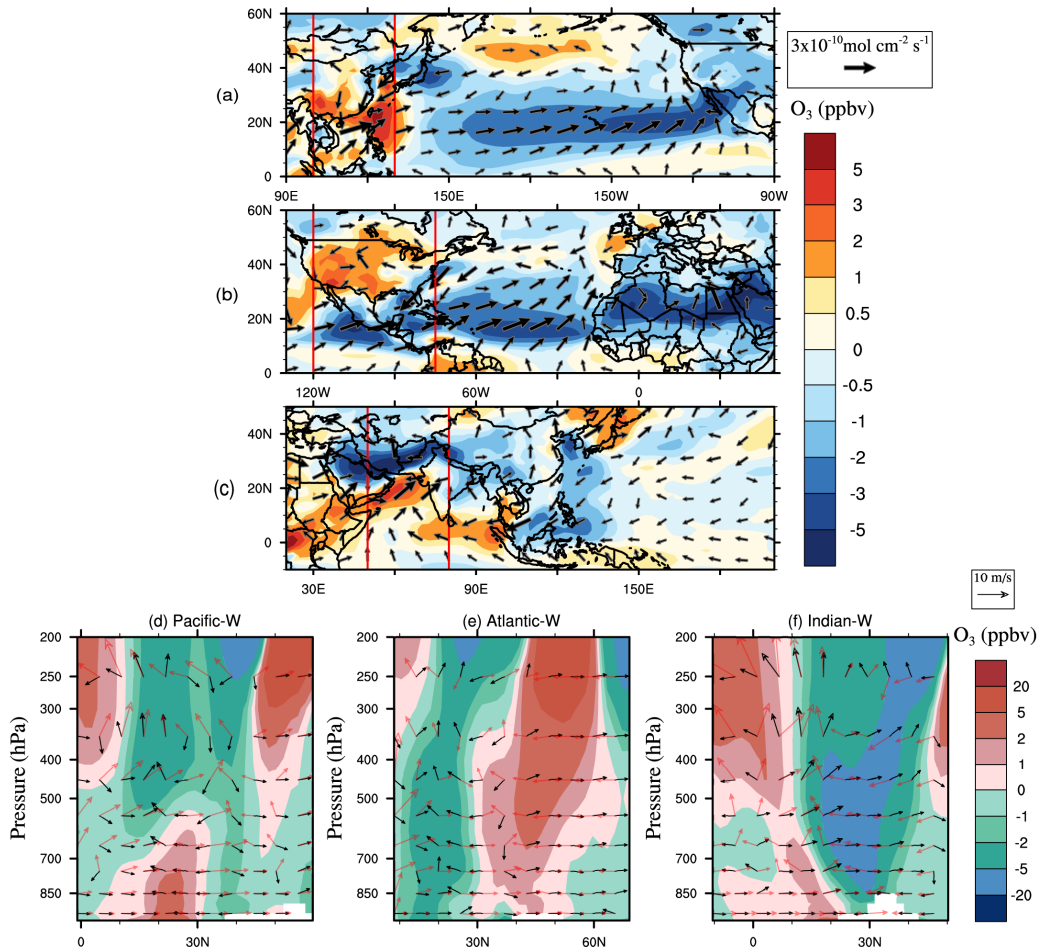
978



979

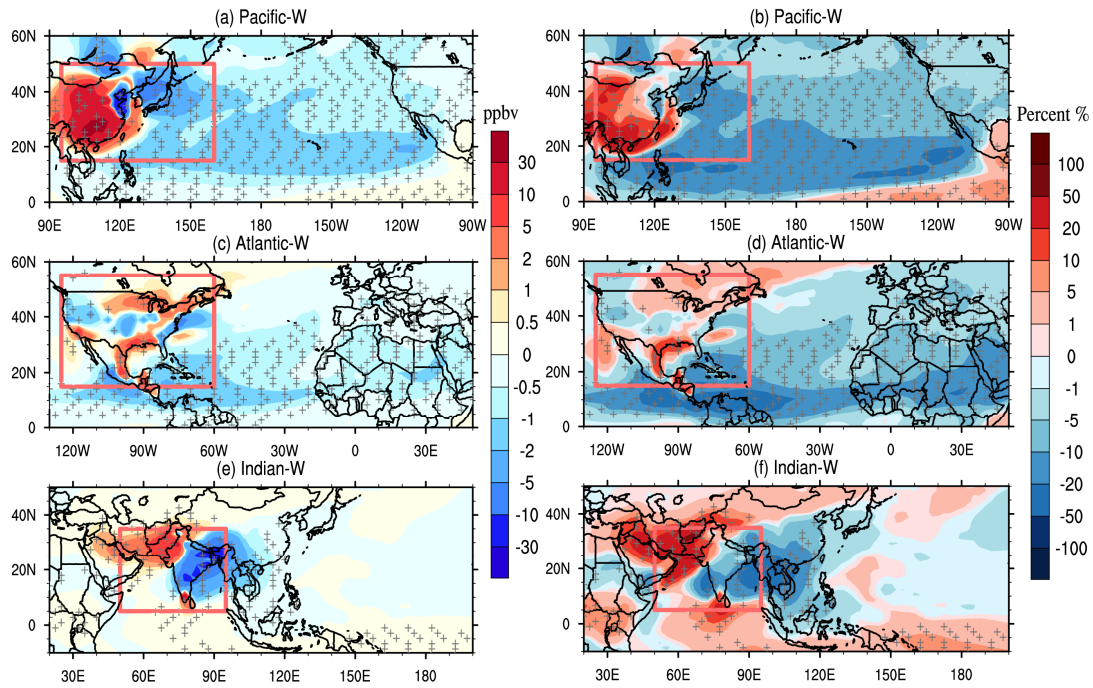
980 **Figure 6.** Spatial pattern of vertical velocity changes at 500 hPa (color contours,  $1 \times 10^{-2}$   
 981  $\text{Pa s}^{-1}$ ) for (a) Pacific-W, (b) Atlantic-W, and (c) Indian-W relative to the CTRL in the  
 982 boreal summer. Positive values indicate upward motion. Red polygons denote the  
 983 regions where the surface pressure responses to SST anomalies are significant (see

984 Figure 5 a-c). The + symbols indicate areas where the results are significant at the 0.05  
 985 level, evaluated by Student's t-test using 20 years of data.  
 986

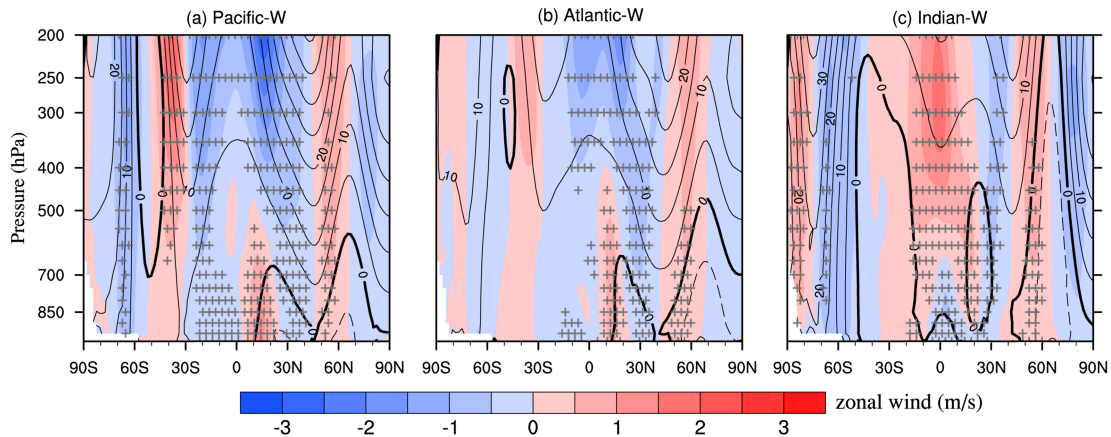


987  
 988 **Figure 7.** Top three rows: Changes in O<sub>3</sub> concentrations (color contours, ppbv) and  
 989 horizontal fluxes (arrows, mol cm<sup>-2</sup> s<sup>-1</sup>) at the surface level for (a) Pacific-W, (b)  
 990 Atlantic-W, (c) Indian-W relative to the CTRL in the boreal summer. Last row: zonal  
 991 average of the tropospheric O<sub>3</sub> changes (color contours, ppbv), wind fluxes in CTRL  
 992 (red arrows, m s<sup>-1</sup>) and the wind flux perturbation (black arrows, m s<sup>-1</sup>) in (d) Pacific-  
 993 W, (e) Atlantic-W, (f) Indian-W relative to the CTRL in the boreal summer. The red  
 994 rectangles in (a), (b) and (c) denote the longitudinal range used for the zonal averages  
 995 in (d), (e) and (f), respectively. The vertical wind velocity is amplified 1000 times to  
 996 make it comparable to the horizontal wind velocity.

997  
 998



999  
 1000 **Figure 8.** Left-hand panel: Difference in the surface concentration (ppbv) of a CO-like  
 1001 tracer emitted from (a) East Asia for Pacific-W, (c) North America for Atlantic-W and  
 1002 (e) the South Asia for Indian-W relative to the CTRL in the boreal summer. Right-hand  
 1003 panel: The percentage changes in the surface concentration of a CO-like tracer emitted  
 1004 from (b) East Asia for Pacific-W, (d) North America for Atlantic-W and (f) South Asia  
 1005 for Indian-W relative to the CTRL in the boreal summer. Red polygons denote the  
 1006 region where the CO-like tracer is emitted from. The + symbol denotes areas where the  
 1007 results are significant at the 0.05 level, evaluated by Student's t-test using 20 years of  
 1008 data.  
 1009



1010  
 1011 **Figure 9.** Zonally averaged changes in zonal wind (color contour, m/s) and geopotential

1012 height (contour, m) for (a) Pacific-W, (b) Atlantic-W and (c) Indian-W relative to the  
1013 CTRL in the boreal summer. Black solid and dashed lines in the contours indicate  
1014 positive and negative geopotential height anomalies, respectively (contour interval: 5  
1015 m). The + symbol denotes areas where the zonal wind changes are significant at the  
1016 0.05 level, evaluated by Student's t-test using 20 years of data.